Article

Synthesis and Reactivity of the Methoxozirconium Pentatungstate (BuN)[{(□-MeO)ZrWO}]: Insights into Proton-Transfer Reactions, Solution Dynamics, and Assembly of {ZrWO} Building Blocks

R. John Errington, Sagar S. Petkar, Paul S. Middleton, William McFarlane, William Clegg, Robert A. Coxall, and Ross W. Harrington

J. Am. Chem. Soc., **2007**, 129 (40), 12181-12196• DOI: 10.1021/ja0725495 • Publication Date (Web): 18 September 2007

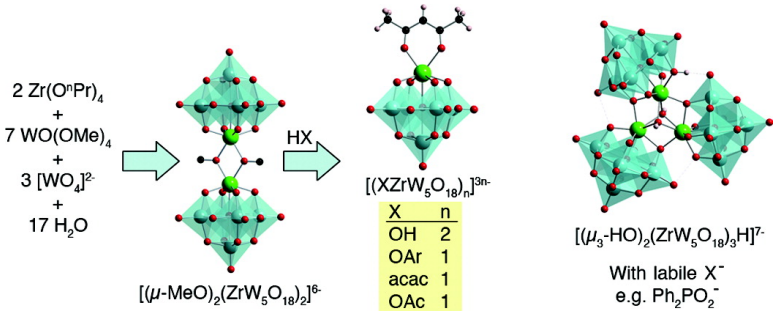

More About This Article

Additional resources and features associated with this article are available within the HTML version:

- Supporting Information
- Links to the 2 articles that cite this article, as of the time of this article download
- Access to high resolution figures
- Links to articles and content related to this article
- Copyright permission to reproduce figures and/or text from this article

View the Full Text HTML

J|A|C|S
ARTICLES
Published on Web 09/18/2007

Synthesis and Reactivity of the Methoxozirconium Pentatungstate (^{n}Bu$_4$N)$_6$[{(μ-MeO)ZrW$_5$O$_{18}$}$_2$]: Insights into Proton-Transfer Reactions, Solution Dynamics, and Assembly of {ZrW$_5$O$_{18}$}$^{2-}$ Building Blocks

R. John Errington,* Sagar S. Petkar, Paul S. Middleton, William McFarlane, William Clegg, Robert A. Coxall, and Ross W. Harrington

Contribution from the School of Natural Sciences, Chemistry, Newcastle University, Newcastle upon Tyne, NE1 7RU, U.K.

Received April 12, 2007; E-mail: John.Errington@ncl.ac.uk

Abstract: The methoxo-bridged, dimeric, Zr^{IV}-substituted Lindqvist-type polyoxometalate (POM) (^{n}Bu$_4$N)$_6$-[{(μ-MeO)ZrW$_5$O$_{18}$}$_2$], (TBA)$_6$**1**, has been synthesized by stoichiometric hydrolysis of Zr(O^{n}Pr)$_4$, [{Zr(O^i-Pr)$_3$(μ-O^{n}Pr)(^{i}PrOH)}$_2$], or [{Zr(O^{i}Pr)$_4$(^{i}PrOH)}$_2$] and [{WO(OMe)$_4$}$_2$] in the presence of (^{n}Bu$_4$N)$_2$WO$_4$, providing access to the systematic nonaqueous chemistry of ZrW$_5$ POMs for the first time and an efficient route to ^{17}O-enriched samples for ^{17}O NMR studies. ^{1}H NMR provided no evidence for dissociation of **1** in solution, although exchange with MeOH was shown to be slow by an EXSY study. Reactions with HX at elevated temperatures gave a range of anions [{XZrW$_5$O$_{18}$}$_n$]$^{3n-}$ (X = OH, **3**; OPh, **4**; OC$_6$H$_4$Me-4, **5**; OC$_6$H$_4$-(CHO)-2, **6**; acac, **7**; OAc, **8**), where $n = 2$ for **3** and $n = 1$ for **4**−**8**, while ^{1}H and ^{17}O NMR studies of hydrolysis of **1** revealed the formation of an intermediate [(μ-MeO)(μ-HO)(ZrW$_5$O$_{18}$)$_2$]$^{6-}$. Electrospray ionization mass spectrometry of **1** and **3** illustrated the robust nature of the ZrW$_5$O$_{18}$ framework, and X-ray crystal structure determinations showed that steric interactions between ligands X and the ZrW$_5$O$_{18}$ surface are important. The coordination number of Zr is restricted to six in aryloxides **4** and **5**, while seven-coordination is achieved in the chelate complexes **6**−**8**. Given the inert nature of the methoxo bridges in **1**, protonation of ZrOW sites is proposed as a possible step in reactions with HX. The diphenylphosphinate ligand in [(Ph$_2$PO$_2$)ZrW$_5$O$_{18}$]$^{3-}$ was found to be labile and upon attempted recrystallization the aggregate [(μ_3-HO)$_2$(ZrW$_5$O$_{18}$)$_3$H]$^{7-}$ **9** was formed, which was found to be protonated at ZrOZr and ZrOW sites. This work demonstrates the flexibility of the {ZrW$_5$O$_{18}$}$^{2-}$ core as a molecular platform for modeling catalysis by tungstated zirconia surfaces.

1. Introduction

The growing importance of polyoxometalates (POMs) in catalysis, as active catalyst components, as catalyst precursors, as supports for immobilized homogeneous catalysts or as molecular models for heterogeneous metal oxide catalysts, has been highlighted in several articles and reviews.[1] These nanoscale molecular metal oxides possess remarkable structural and compositional diversity which, coupled with their Brønsted acid and redox properties, provides an attractive platform for catalyst development, but despite their widespread use as Brønsted acid and oxidation catalysts their full potential has yet to be realized.

Heterometallic POMs are of particular interest as they provide a unique opportunity to study at the molecular level the reactivity of isolated heterometal sites embedded within a matrix of another metal oxide and, hence, to establish a basis for understanding the activity of mixed oxide catalysts. Tungsten oxide supported on titanium or zirconium oxide is strongly acidic, and studies of WO_3/ZrO_2 and WO_3/TiO_2 catalysts have led to the intriguing suggestion that Brønsted acid activity in these systems is associated with the formation of polynuclear oxotungsten aggregates, possibly with heterometal incorporation, at the surface of these materials.[2] These studies have identified zirconia-supported tungsten oxide as a promising catalyst for the isomerization of light alkanes to high octane gasoline, offering major environmental benefits over conventional processes which use mainly chlorinated liquid or solid catalysts. Solid acid polyoxometalates have been found to be similarly active as catalysts for hydrocarbon transformations, and *ab initio*

(1) For recent reviews of catalysis involving polyoxometalates, see: (a) Hill, C. L., Ed. *J. Mol. Catal. A: Chem.* **2007**, *262*, 1−242. This special issue is dedicated to polyoxometalate catalysis. (b) Hill, C. L. *J. Mol. Catal. A: Chem.* **2007**, *262*, 2−6 and references therein. This article provides a convenient summary of previous leading reviews on catalysis involving polyoxometalates.

(2) (a) Hino, M.; Arata, K. *J. Chem. Soc., Chem. Commun.* **1988**, 1259−1260. (b) Barton, G. B.; Soled, S. L.; Iglesia, E. *Top. Catal.* **1998**, *6*, 87−99. (c) Scheithauer, M.; Grasselli, R. K.; Knözinger, H. *Langmuir* **1998**, *14*, 3019−3029. (d) Scheithauer, M.; Cheung, T.-K.; Jentoft, R. E.; Grasselli, R. K.; Gates, B. C.; Knözinger, H. *J. Catal.* **1998**, *180*, 1−13. (e) Barton, D. G.; Soled, S. L.; Metzner, G. D.; Fuentes, G. A.; Iglesia, E. *J. Catal.* **1999**, *181*, 57−72. (f) Barton, G. B.; Shtein, M.; Wilson, R. D.; Soled, S. L.; Iglesia, E. *J. Phys. Chem. B* **1999**, *103*, 630−640. (g) Eibl, S.; Gates, B. C.; Knözinger, H. *Langmuir* **2001**, *17*, 107−115. (h) Valigi, M.; Gazzoli, D.; Pettiti, I.; Mattei, G.; Colonna, S.; De Rossi, S.; Ferraris, G. *App. Catal. A* **2002**, *231*, 159−172. (i) Kuba, S.; Lukinskas, P.; Grasselli, R. K.; Gates, B. C.; Knözinger, H. *J. Catal.* **2003**, *216*, 353−361. (j) Onfroy, T.; Guillaume, C.; Houalla, M. *J. Phys. Chem. B* **2005**, *109*, 3345−3354.

studies of reactions between protonated $[PW_{12}O_{40}]^{3-}$ and alkenes have shown that activation barriers for the formation of surface alkoxides in this system are lower than those for similar reactions on zeolites.[3] It therefore follows that alkoxide derivatives of mixed Zr/W POMs should provide an opportunity to develop a molecular level understanding of reactions occurring on zirconia-supported tungsten oxide catalysts, but until recently very few examples of polytungstates containing Zr addenda atoms within the oxide framework had been reported, none of which contained alkoxide ligands and most were derivatives of Keggin or Wells−Dawson structures.[4]

Our initial attempt to prepare the tetrabutylammonium (TBA) salt of the Lindqvist-type anion $[(MeO)ZrW_5O_{18}]^{3-}$ **1** using a method analogous to that used for $[(MeO)TiW_5O_{18}]^{3-}$ **2** gave an ill-defined product,[5] while a zirconotungstate obtained by Chauveau et al. from a reaction between acidified aqueous solutions of $[WO_4]^{2-}$ and $ZrOCl_2{\cdot}8H_2O$ in the presence of $[SO_4]^{2-}$ was formulated as $[(H_2O)ZrW_5O_{18}]^{2-}$ where one of the $\{W{=}O\}^{4+}$ groups in $[W_6O_{19}]^{2-}$ had been replaced by $\{Zr(H_2O)\}^{4+}$,[6] although ^{183}W NMR data were somewhat ambiguous and a crystal structure was not determined. More recently, Villanneau and co-workers have determined the structures of DMSO derivatives $[(DMSO)_n(H_2O)_{3-n}ZrW_5O_{18}]^{2-}$ ($n = 1, 2$) in which the Zr is eight-coordinate and accordingly reformulated the Chauveau anion as $[(H_2O)_3ZrW_5O_{18}]^{2-}$.[7] During the course of our work, this group also reported the preparation and structural characterization of the hydrated TBA salt of the dimeric hydroxo zirconotungstate $[\{(\mu\text{-HO})ZrW_5O_{18}\}_2]^{6-}$ **3**, which they obtained from $[(H_2O)_3ZrW_5O_{18}]^{2-}$ by treatment with (TBA)OH.[8]

We have developed nonaqueous syntheses of Lindqvist-type alkoxo heterometalates $[(RO)MW_5O_{18}]^{n-}$ from mixtures of WO_4^{2-} and the constituent metal alkoxides, where M is a group 4 or 5 transition metal.[5] By controlling the extent of hydrolysis a single alkoxide site can be retained at the heterometal, enabling reactivity studies and systematic variation in surface functionality. An additional advantage of this preparative method is that ^{17}O-enriched samples for solution NMR studies are readily obtained using only stoichiometric amounts of ^{17}O-enriched water for the hydrolysis. Of the Group 4 derivatives, the titanium methoxide $[(MeO)TiW_5O_{18}]^{3-}$ **2** was fully characterized, including its crystal structure, but the nature of the analogous zirconium compound remained somewhat ambiguous, presumably because of ill-defined alkoxide groups. However, after refining the synthetic procedure we now have a reliable route to the first example of an alkoxo zirconotungstate $[\{(\mu\text{-MeO})ZrW_5O_{18}\}_2]^{6-}$ **1**, the structure of which we previously communicated only briefly.[9] We describe here the synthesis and structure of **1** and systematic reactions with protic reagents HX to give the dimeric hydroxide **3** and the first structurally characterized series of monomeric derivatives $[(X)ZrW_5O_{18}]^{3-}$ (X = OC_6H_5 **4**, OC_6H_4Me-4 **5**, OC_6H_4CHO-2 **6**, acac **7**, OAc **8**) as shown in Scheme 1. The structure of the novel protonated aggregate $[(\mu_3\text{-HO})_2\{ZrW_5O_{18}\}_3H]^{7-}$ **9**, which was obtained from the attempted preparation of the diphenylphosphinate derivative $[(Ph_2PO_2)ZrW_5O_{18}]^{3-}$, is also described. Results from ^1H and ^{17}O NMR studies of **1** and **3** and their methanolysis and hydrolysis reactions are presented, and implications for dynamic solution behavior and reaction mechanisms are discussed.

Scheme 1. Preparative Routes to Anions **1** and **3**−**8**

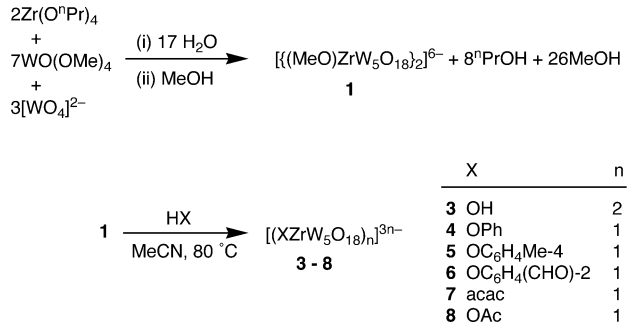

2. Results

Synthesis and Characterization of $(TBA)_6$1. Our first attempts to synthesize the alkoxozirconium Lindqvist anion $[(MeO)ZrW_5O_{18}]^{3-}$ from $(TBA)_2WO_4$, $WO(OMe)_4$, and $Zr(O^nPr)_4$ gave an ill-defined product, which appeared to be a mixture of ZrW_5 species with different alkoxide substituents, and we were unable to obtain crystals for a single-crystal X-ray structure determination.[5] We subsequently established that complete exchange of any residual O^nPr groups could be achieved by treating the initial product from the hydrolysis reaction with an excess of MeOH to give good yields of methoxide $(TBA)_6$**1** after recrystallization from acetonitrile−ether to remove small amounts of $(TBA)_2[W_6O_{19}]$. The better defined zirconium alkoxides $[\{Zr(O^iPr)_4(^iPrOH)\}_2]$ and $[\{Zr(O^iPr)_3(\mu\text{-}O^nPr)(^iPrOH)\}_2]$ were also used in the reaction, although yields were not greatly affected. The ^{183}W NMR spectrum of **1** is typical of a substituted MW_5 Lindqvist structure,[5,7,8] with a peak at 37.6 for the four equatorial tungstens and a smaller peak at 64.4 ppm due to the single axial tungsten. The ^{17}O NMR spectrum of $(TBA)_6$**1** with a small amount of hexatungstate impurity is shown in Figure 1, and the six peaks associated with the ZrW_5O_{18} oxide framework are readily assigned, *viz.* two peaks in the terminal W=O region at 711 and 691 ppm (a and b), one peak for bridging ZrOW at 484 ppm (c), two peaks for bridging WOW at 385 and 377 ppm (d and e, although it was not possible to differentiate between these sites), and one peak for the central μ_6-O at −58 ppm (f). Terminal W=O and bridging WOW peaks for **1** are significantly broader than those for $[W_6O_{19}]^{2-}$ while peaks for ZrOW and μ_6-O remain comparatively sharp. ^{17}O NMR line widths are determined

(3) Campbell, K. A.; Janik, M. J.; Davis, R. J.; Neurock, M. *Langmuir* **2005**, *21*, 4738−4745.
(4) (a) Finke, R. G.; Rapko, B.; Weakley, T. J. R. *Inorg. Chem.* **1989**, *28*, 1573−1579. (b) Gaunt, A. J.; May, I.; Collinson, D.; Holman, K. T.; Pope, M. T. *J. Mol. Struct.* **2003**, *656*, 101−106. (c) Gaunt, A. J.; May, I.; Collinson, D.; Helliwell, M. *Acta Crystallogr., Sect. C* **2003**, *59*, i65−i66. (d) Fang, X.; Anderson, T. M.; Hou, Y.; Hill, C. L. *Chem. Commun.* **2005**, 5044−5046. (e) Fang, X.; Anderson, T. M.; Hill, C. L. *Angew. Chem., Int. Ed.* **2005**, *44*, 3540−3544. (f) Bassil, B. S.; Dickman, M. H.; Kortz, U. *Inorg. Chem.* **2006**, *45*, 2394−2396. (g) Kholdeeva, O. A.; Maksimov, G. M.; Maksimovskaya, R. I.; Vanina, M. P.; Trubitsina, T. A.; Naumov, D. Y.; Kolesov, B. A.; Antonova, N. S.; Carbó, J. J.; Poblet, J. M. *Inorg. Chem.* **2006**, *45*, 7244−7234. (h) Kato, C. N.; Shinohara, A.; Hayashi, K.; Nomiya, K. *Inorg. Chem.* **2006**, *45*, 8108−8119.
(5) Clegg, W.; Elsegood, M. R. J.; Errington, R. J.; Havelock, J. *J. Chem. Soc., Dalton Trans.* **1996**, 681−690.
(6) Chauveau, F.; Eberle, J.; Lefebvre, J. *Nouv. J. Chim.* **1985**, *9*, 315−320.
(7) Carabineiro, H.; Villanneau, R.; Carrier, X.; Herson, P.; Lemos, F.; Ramôa Ribeiro, F.; Proust, A.; Che, M. *Inorg. Chem.* **2006**, 1915−1923.
(8) Villanneau, R.; Carabineiro, H.; Carrier, X.; Thouvenot, R.; Herson, P.; Lemos, F.; Ramôa Ribeiro, F. R.; Che, M. *J. Phys. Chem. B* **2004**, *108*, 12465−12471.
(9) Errington, R. J. In *Polyoxometalate Molecular Science*; Borrás-Almenar, J. J., Coronado, E., Müller, A., Pope, M. T., Eds.; Kluwer: Dordrecht, The Netherlands, 2003; pp 55−77.

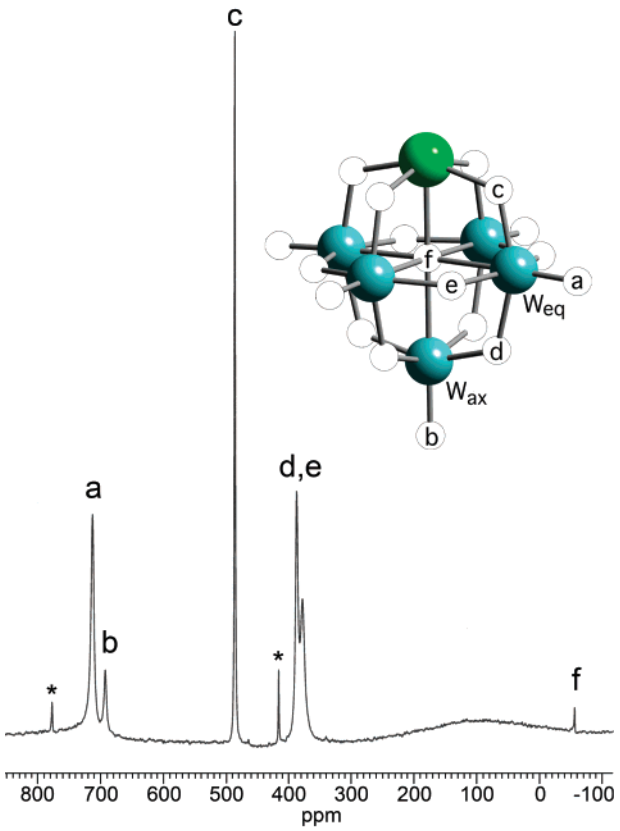

Figure 1. ^{17}O NMR spectrum of **1** in MeCN and diagram of the ZrW_5O_{18} cage. Peaks due to $[W_6O_{19}]^{2-}$ impurity are marked with an asterisk.

predominantly by quadrupolar relaxation, although metal−oxygen spin−spin coupling and chemical exchange may also contribute.

$$\frac{1}{T_1} = \frac{3}{125}\left(1 + \frac{\eta^3}{3}\right)\left(\frac{e^2qQ}{\hbar}\right)^2 \tau_c \qquad (1)$$

For rapid, isotropic molecular tumbling, the quadrupolar relaxation time T_1 for ^{17}O is determined by eq 1,[10] where η is the electric field asymmetry parameter, Q is the nuclear electric quadrupole moment, q is the largest component of the electric field gradient, and τ_c is the correlation time for molecular rotation. The dimeric anion **1** is larger than $[W_6O_{19}]^{2-}$ and is likely to undergo anisotropic rotation in solution, giving rise to longer correlation times and broader lines than those for the symmetric $[W_6O_{19}]^{2-}$, although the sharper lines for O_c and O_f suggest that electric field gradients at these nuclei are smaller than those at $O_{a,b}$ and $O_{d,e}$. Klemperer has shown that quadrupole moments for ^{93}Nb ($I = {}^9/_2$, 100% natural abundance) and ^{51}V ($I = {}^7/_2$, 99.76% natural abundance) of −0.22 and −0.05, respectively, are not sufficiently large to cause rapid quadrupolar relaxation and spin−spin decoupling of the metal nuclei, and unresolved coupling leads to severe line broadening for oxygens bonded to these metals in $[NbW_5O_{19}]^{3-}$ and $[VW_5O_{19}]^{3-}$.[11,12] The quadrupole moment of ^{91}Zr ($I = {}^5/_2$, 11.23% natural abundance) is similar to that of ^{93}Nb, but the natural abundance is too small to cause any significant broadening in the ^{17}O NMR spectrum of **1** through spin−spin coupling. The possibility that the line broadening is caused by dynamic solution behavior is discussed later in Section 3.

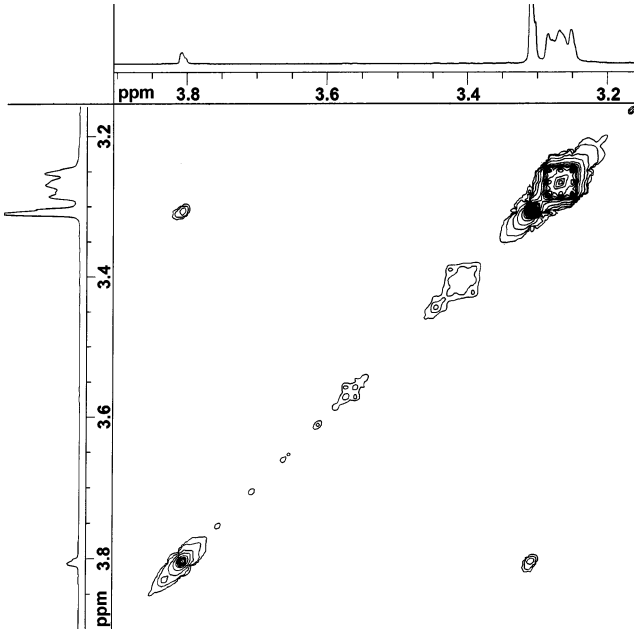

Figure 2. Part of the 2D ^{1}H EXSY NMR spectrum of a mixture of $(TBA)_6$**1** and MeOH at 75 °C in CD_3CN showing exchange between ZrOMe at 3.81 and MeOH at 3.31 ppm.

^{1}H and ^{13}C{^{1}H} NMR spectra of $(TBA)_6$**1** contained methoxide singlets at 3.74 and 59.1 ppm, respectively, which are both upfield of the corresponding peaks for terminal TiOMe in **2**, which appear at 4.10 and 62.35 ppm, respectively.[5] Upfield shifts have also been observed for bridging methoxides in dimeric $[\{WO(OMe)_4\}_2]$[13] and $[\{M(OMe_5)\}_2]$ (M = Nb, Ta),[14] which both display dynamic solution behavior involving initial cleavage of one of the methoxide bridges. An X-ray crystal structure determination showed that **1** was indeed dimeric with bridging methoxides (see below), and in a variable-temperature ^{1}H NMR study from ambient temperature to 75 °C the methoxide peak shifted slightly downfield to 3.80 ppm but remained sharp, suggesting that any dissociation into monomeric $[(MeO)ZrW_5O_{18}]^{3-}$ with terminal methoxide is slow over this temperature range.

Methoxide Exchange between 1 and Methanol. To explore further the lability of the Zr−OMe bonds in **1**, the exchange reaction with MeOH was monitored by ^{1}H NMR spectroscopy. A mixture of $(TBA)_6$**1** and MeOH showed separate, sharp ^{1}H NMR resonances for ZrOMe and MeOH at temperatures up to 75 °C, indicating that exchange is slow on the NMR time scale even at elevated temperatures. However, a two-dimensional ^{1}H EXSY NMR experiment (Figure 2) demonstrated that slow exchange does occur with an exchange rate of 0.03 s^{-1} at 75 °C.

Hydrolysis of 1. We have previously shown that the methoxide-substituted NbW_5 Lindqvist anion $[(MeO)NbW_5O_{18}]^{2-}$ is readily hydrolyzed to give the oxo-bridged $[\{(\mu\text{-O})NbW_5O_{18}\}_2]^{4-}$.[5] In contrast, hydrolysis of $(TBA)_6$**1** ultimately produced the hydroxide-bridged dimer $(TBA)_6$**3**, which gave a

(10) Abragam, A. *The Principles of Nuclear Magnetism*; Oxford University Press: London, 1961; p 314.
(11) Besecker, C. J.; Klemperer, W. G.; Maltbie, D. J.; Wright, D. A. *Inorg. Chem.* **1985**, *24*, 1027−1032.
(12) Filowitz, M.; Ho, R. K. C.; Klemperer, W. G.; Shum, W. *Inorg. Chem.* **1979**, *18*, 93−103.
(13) Clegg, W.; Errington R. J.; Kraxner, P.; Redshaw, C. *J. Chem. Soc., Dalton Trans.* **1992**, 1431−1438.
(14) Bradley, D. C.; Holloway, C. E. *J. Chem. Soc. A* **1968**, 219−223.

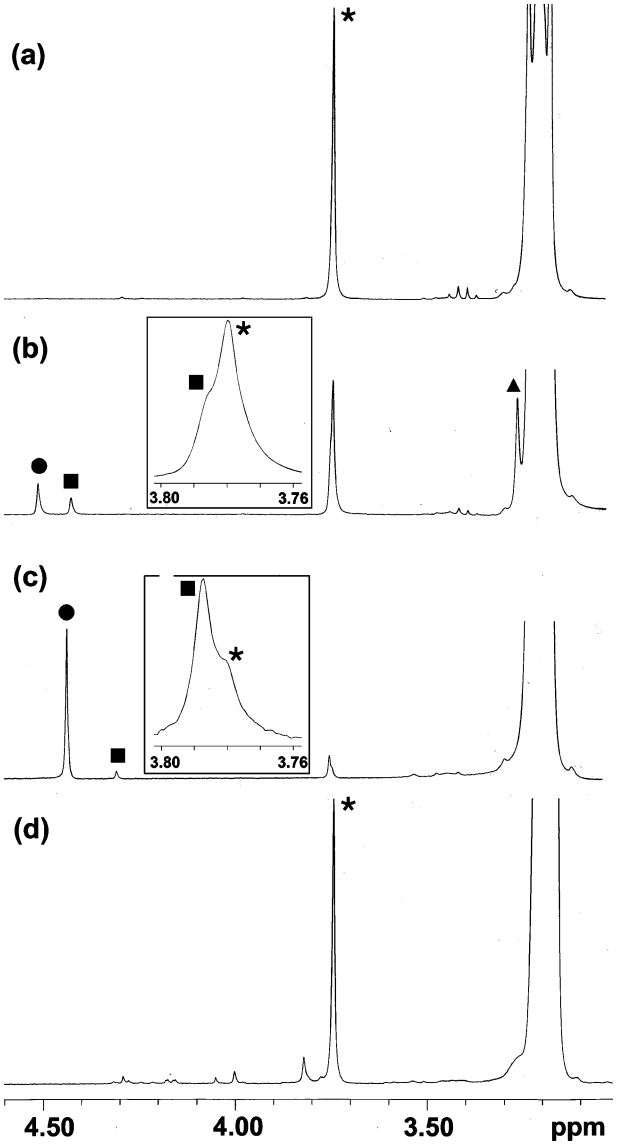

Figure 3. ^{1}H NMR spectra from a study of the hydrolysis of $(TBA)_6$**1**: before addition of H_2O (a); 2 h after addition of 1 equiv of H_2O (b); after reflux and removal of volatiles (c); after treatment of the hydrolyzed product with MeOH and removal of volatiles (d). Inserts show expansion of the methoxide region. Peaks are assigned as **1** (★), $[\{(\mu\text{-HO})(\mu\text{-MeO})ZrW_5O_{18}\}_2]^{6-}$ (■), **3** (●), and MeOH (▲). Note OH peaks are solvent-sensitive and move to a lower frequency upon removal of MeOH and H_2O.

peak in the ^{1}H NMR spectrum at 4.43 ppm, although a μ-OH resonance could not be assigned unambiguously in the ^{17}O NMR spectrum. Metal oxide framework peaks in the ^{17}O NMR spectrum of **3** had similar chemical shifts to those for **1**, except that the single ZrOW peak was shifted slightly upfield to 478 ppm.

A more detailed ^{1}H NMR study of the hydrolysis of **1** (Figure 3) showed that equilibrium was reached after about 2 h at approximately 60% conversion, whereupon two OH peaks, a new OMe peak, and a MeOH peak had appeared in the spectrum. Heating the sealed NMR sample at 80 °C for 4 h made little difference to the ^{1}H NMR spectrum, but after overnight reflux and removal of the volatiles, the product was a mixture of **1** (2%), **3** (88%), and an intermediate hydrolysis product formulated as $[\{(\mu\text{-HO})(\mu\text{-MeO})ZrW_5O_{18}\}_2]^{6-}$ (10%), with characteristic OH and OMe peaks at 4.30 and 3.774 ppm, respectively. After removal of the solvent, treatment of this mixture with an excess of MeOH under reflux gave back the

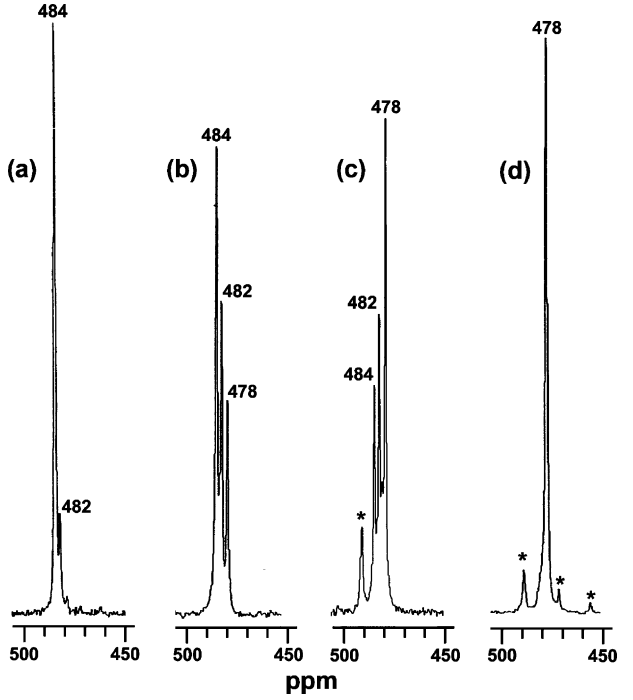

Figure 4. ZrOW region of ^{17}O NMR spectra of $[\{(MeO)ZrW_5O_{18}\}_2]^{6-}$ (a); mixtures of $[\{(MeO)ZrW_5O_{18}\}_2]^{6-}$, $[\{(\mu\text{-HO})(\mu\text{-MeO})ZrW_5O_{18}\}_2]^{6-}$, and $[\{(HO)ZrW_5O_{18}\}_2]^{6-}$ (b and c); and $[\{(HO)ZrW_5O_{18}\}_2]^{6-}$ (d). Impurity peaks are marked with an asterisk.

methoxide **1** together with minor amounts of other methoxide species as shown in Figure 3d. The comparatively sharp peaks in the ZrOW region of ^{17}O NMR spectra were also useful in monitoring hydrolysis, and the ZrOW peak at 482 ppm in the spectra of partially hydrolyzed samples (Figure 4) was assigned to the intermediate $[\{(\mu\text{-HO})(\mu\text{-MeO})ZrW_5O_{18}\}_2]^{6-}$.

Oxygen Exchange between 3 and Water. Complete conversion of **1** to **3** on a preparative scale was achieved by treating $(TBA)_6$**1** with an excess of water at 80 °C for 30 min, removing the volatiles and repeating this hydrolysis procedure twice more. ^{1}H NMR spectra gave the correct relative integrations for OH and NCH_2 peaks, although ^{17}O NMR showed that the hydrolyzed product contained small amounts of $[W_{10}O_{32}]^{4-}$. In addition, the ^{17}O NMR spectrum of the product showed that much of the ^{17}O enrichment in **3** had been lost, confirming that oxygen exchange occurs between water and the oxometalate cage. A sample of **3** prepared by this route was therefore treated with an excess of 10% ^{17}O-enriched water, and the ^{17}O NMR spectrum was monitored while heating to 50 °C in order to investigate the oxygen exchange process. Upon mixing, a broad peak appeared at 177 ppm in the ^{17}O NMR spectrum at ambient temperature as shown in Figure 5a. After heating to 50 °C, the peaks due to **3** became much more intense relative to the broad peak, which shifted slightly upfield to 174 ppm, and after 30 min at 50 °C the WOW peak at 380 ppm had become more intense than the other peaks in the spectrum. The $[W_{10}O_{32}]^{4-}$ impurity was not enriched under these conditions. A peak at about 180 ppm in the ^{17}O NMR spectrum of aqueous $[Zr_4(OH)_8(H_2O)_{16}]^{8+}$ was assigned to slowly exchanging water,[15] suggesting that the broad peak at 177 ppm in Figure 5 could be due to zirconium-bound water which is slowly exchanging with noncoordinated water and with ZrOH, and implying cleavage

(15) Åberg, M.; Glaser, J. *Inorg. Chim. Acta* **1993**, *206*, 53−61.

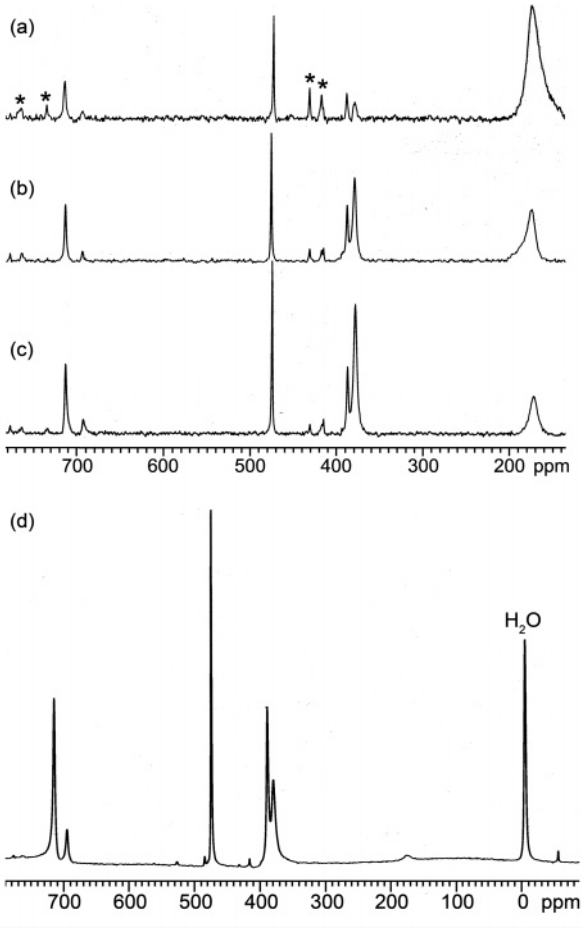

Figure 5. ^{17}O NMR spectra of exchange reaction between (TBA)$_6$**3** (0.057 mmol) and ^{17}O enriched water (0.259 mmol ^{17}O) after 15 min at 21 °C (a), after heating to 50 °C (b), after 30 min at 50 °C (c), and after 2 weeks at ambient temperature (d). Peaks marked with an asterisk are due to [W$_6$O$_{19}$]$^{2-}$ and [W$_{10}$O$_{32}$]$^{4-}$ impurities.

of one or both of the Zr-(μ-OH) bonds in **3** to give asymmetric Zr_2W_{10} or monomeric ZrW_5 intermediates with bound water. Alternatively, the peak at 177 ppm may indicate the formation of a small amount of $[Zr_4(OH)_8(H_2O)_{16}]^{8+}$. Although we were unable to assign a peak to ZrOH in the ^{17}O NMR spectrum of **3**, the intensity of the peak at 380 ppm in Figure 5c may indicate that the OH resonance is coincident with the upfield WOW peak at this temperature. Figure 5d shows the ^{17}O NMR spectrum after 2 weeks at ambient temperature, when about 67% of the ^{17}O from the enriched water had been transferred to the oxometalate, but there is still no peak which can be unambiguously assigned to ZrOH.

After prolonged hydrolysis of (TBA)$_6$**1** at elevated temperatures the ^{17}O NMR spectrum of the product contained minor peaks for [W$_6$O$_{19}$]$^{2-}$ at 775 (W═O), 414 (WOW), and −81 (μ$_6$-O) ppm and for [W$_{10}$O$_{32}$]$^{4-}$ at 762 and 733 (W═O), 430 and 416 (WOW), and −6 (μ$_5$-O) ppm in addition to those of **3**. Remarkably, given the small amounts of these impurities, single crystals were obtained from this product which contained all three POMs (TBA)$_2$[W$_6$O$_{19}$], (TBA)$_4$[W$_{10}$O$_{32}$], and (TBA)$_6$**3** (see below). This degradation of the ZrW_5O_{18} framework may be associated with the peak in the exchange study described above that could be due to $[Zr_4(OH)_8(H_2O)_{16}]^{8+}$, in which case it would essentially be the reverse of the aqueous preparation

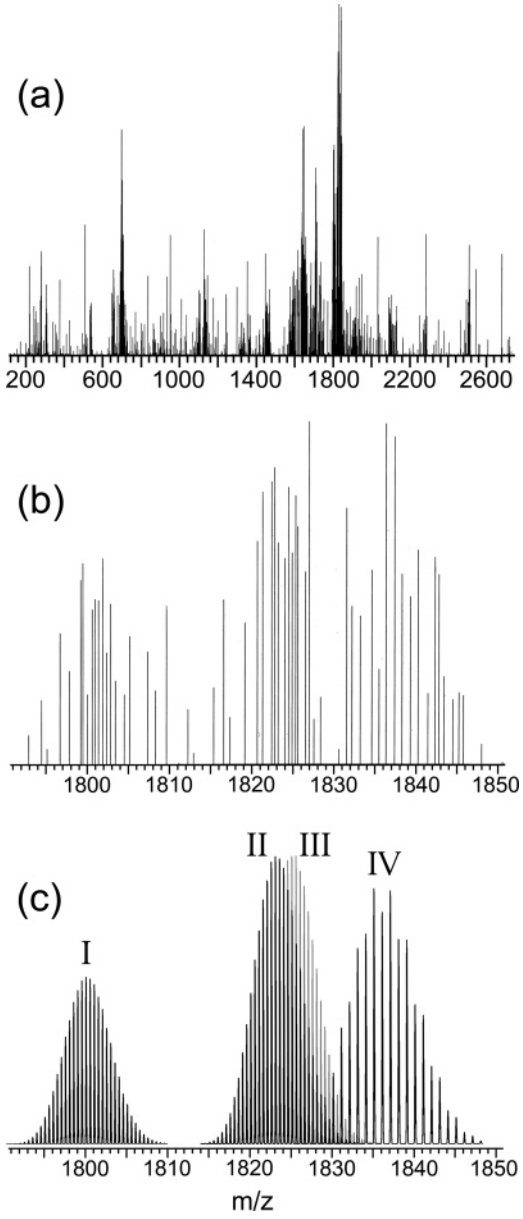

Figure 6. (a) Negative ion ESI mass spectrum of (TBA)$_6$**1**, (b) expansion of ESI mass spectrum of (TBA)$_6$**1** in the *m*/*z* range 1800−1850, (c) ion cluster patterns for {(TBA)$_4$[(HO)$_2$(ZrW$_5$O$_{18}$)$_2$]}$^{2-}$ (I), {(TBA)$_4$[(MeO)$_2$-(ZrW$_5$O$_{18}$)$_2$](H$_2$O)}$^{2-}$ (II), {(TBA)$_4$[(MeO)(HO)(ZrW$_5$O$_{18}$)$_2$](H$_2$O)$_2$}$^{2-}$ (III), and {(TBA)$_2$[(H$_2$O)$_2$(HO)(ZrW$_5$O$_{18}$)]}$^{-}$ (IV) calculated using iMass.

of $[(H_2O)_3ZrW_5O_{18}]^{2-}$ from $[W_{10}O_{32}]^{4-}$ and $[Zr_4(OH)_8(H_2O)_{16}]^{8+}$.[6,7]

Electrospray Ionization (ESI) Mass Spectrometry of 1 and 3. The most intense ion cluster peaks in the negative-ion ESI mass spectra of (TBA)$_6$**1** and (TBA)$_6$**3** can be assigned to either dimeric or monomeric species containing the ZrW_5O_{18} core. The ESI mass spectrum of (TBA)$_6$**1** is shown in Figure 6 together with an expansion of the *m*/*z* region between 1800 and 1850 and calculated ion cluster peaks for this region. Tables 1 and 2 list peak assignments for the mass spectra of (TBA)$_6$**1** and (TBA)$_6$**3**, respectively, although in some cases assignments are ambiguous because of possible proton redistribution between methoxide and water or hydroxide and methanol. Several peaks in the mass spectrum of (TBA)$_6$**1** arise from hydrolysis, two of which are also present in the mass spectrum of (TBA)$_6$**3**, while

Table 1. Peak Assignments for the Negative-Ion Electrospray Ionization Mass Spectrum of $(TBA)_6$**1**

ion	monoisotopic *m/z*	observed *m/z*
$\{H[(HO)(ZrW_5O_{18})]\}^{2-}$	657.8	655
$\{H[(MeO)(ZrW_5O_{18})](MeOH)_2\}^{2-}$	696.8	696
$\{(TBA)_2H_2[(MeO)_2(ZrW_5O_{18})_2](MeOH)_4\}^{2-}$	1635.9	1638
$\{(TBA)_2H_2[(MeO)_2(ZrW_5O_{18})_2](MeOH)_4(H_2O)\}^{2-}$ or $\{(TBA)_2H_2[(MeO)(HO)(ZrW_5O_{18})_2](MeOH)_5\}^{2-}$	1644.9	1644
$\{(TBA)_3H[(MeO)_2(ZrW_5O_{18})_2](MeOH)\}^{2-}$	1708.5	1709
$\{(TBA)_3H[(MeO)_2(ZrW_5O_{18})_2](MeOH)_2(H_2O)\}^{2-}$ or $\{(TBA)_3H[(MeO)(HO)(ZrW_5O_{18})_2](MeOH)_3\}^{2-}$	1733.6	1733
$\{(TBA)_4[(HO)_2(ZrW_5O_{18})_2]\}^{2-}$	1799.1	1802
$\{(TBA)_4[(MeO)_2(ZrW_5O_{18})_2](H_2O)\}^{2-}$ or $\{(TBA)_4[(MeO)(HO)(ZrW_5O_{18})_2](MeOH)\}^{2-}$	1822.1	1822
$\{(TBA)_4[(MeO)(HO)(ZrW_5O_{18})_2](H_2O)_2\}^{2-}$	1824.1	1824
$\{(TBA)_2[(HO)(ZrW_5O_{18})](H_2O)_2\}^{-}$	1835.2	1836

Table 2. Peak Assignments for the Negative Ion Electrospray Ionization Mass Spectrum of $(TBA)_6$**3**

ion	monoisotopic *m/z*	observed *m/z*
$\{H[(HO)(ZrW_5O_{18})]\}^{2-}$	657.8	655
$\{H[(HO)(ZrW_5O_{18})](H_2O)_4\}^{2-}$	693.8	694
$\{(TBA)_2H_2[(HO)_2(ZrW_5O_{18})_2](H_2O)_6\}^{2-}$	1619.9	1618
$\{(TBA)_3H[(HO)_2(ZrW_5O_{18})_2](H_2O)_4\}^{2-}$	1714.5	1716
$\{(TBA)_4[(HO)_2(ZrW_5O_{18})_2]\}^{2-}$	1799.1	1803
$\{H_5[(HO)_2(ZrW_5O_{18})_2](H_2O)_4\}^{-}$	2706.2	2708

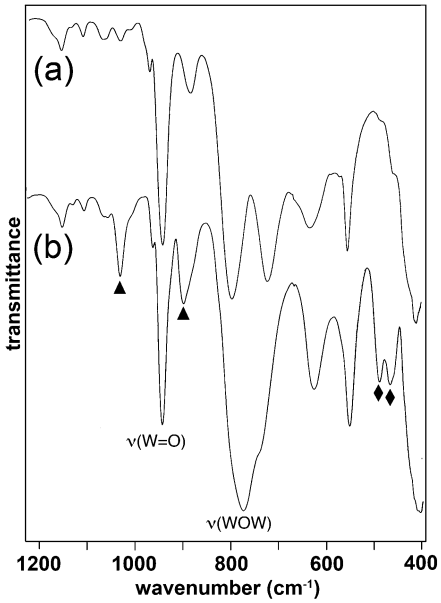

Figure 7. FTIR spectra in the range 400−1200 cm^{-1} of $(TBA)_6$**3** (a) and $(TBA)_6$**1** (b) as powders on a single reflection ATR cell. Bands marked with ▲ are assigned to ν(C−O), and those with ◆, to ν(Zr−OC).

others can be formulated as ions derived from the intermediate hydrolysis product $[(MeO)(HO)(ZrW_5O_{18})_2]^{6-}$.

FTIR Spectra of 1 and 3. Substitution of $[Zr{-}X]^{3+}$ for $[W{=}O]^{4+}$ in the Lindqvist anion $[W_6O_{19}]^{2-}$ lowers the symmetry from O_h and splits the bands due to ν(WO) in the FTIR spectra of **1** and **3** (Figure 7). In addition, due to the higher anionic charge of the resulting ZrW_5 units, a bathochromic shift is observed for W−O vibrations compared to those for $[W_6O_{19}]^{2-}$. Hence, ν(W=O) bands for **1** were observed at 943 and 963 cm^{-1} compared to the single ν(W=O) band for $[W_6O_{19}]^{2-}$ at 974 cm^{-1}. Similarly, ν(WO) bands for bridging oxygens were observed at 774 and 740 cm^{-1} compared to the single band at 814 cm^{-1} for $[W_6O_{19}]^{2-}$. Similar shifts have been observed in IR spectra of other heterometallic Lindqvist structures.[16] By comparing the IR spectrum of **1** with that of **3** and with reference to an earlier study of infrared spectra of zirconium compounds with bridging ethoxides,[17] we are able to assign bands at 1031 and 898 cm^{-1} to ν(C−O) of the methoxide ligand, in comparison with the value of 1012 cm^{-1} reported for the bridging methoxide in $[Nb_2W_4O_{19}CH_3]^{3-}$,[18] and bands at 489 and 467 cm^{-1} to ν(Zr−OC). An adjustment for the reduced mass in the OH bridges in **3** indicates that the band at 723 cm^{-1} in the infrared spectrum of **3** is due to ν(Zr−OH), which is consistent with Kholdeeva's suggestion that the band at *ca.* 770 cm^{-1} in the IR spectra of $[(\mu\text{-}OH)_2(ZrPW_{11}O_{39})_2]^{8-}$ is due to the Zr−(OH)−Zr bonds.[4(g)]

Electrochemistry of 1. The hexatungstate $(TBA)_2[W_6O_{19}]^{2-}$ undergoes a reversible one-electron reduction in acetonitrile with a further reduction at a more negative potential close to the solvent limit, although careful control of solvent purity is necessary for observation of the second reduction wave.[19,20] In contrast, we were unable to observe any reduction of a 0.005 M solution of $(TBA)_6$**1** in acetonitrile by cyclic voltammetry. This presumably reflects the higher anionic charge associated with each ZrW_5 unit in **1** which makes reduction to $[(MeO)_2(ZrW_5O_{18})_2]^{7-}$ more difficult, as is the case in the reduction of $[W_6O_{19}]^{3-}$ to $[W_6O_{19}]^{4-}$. Ion pairing between Li^+ and POMs has been reported to shift reduction potentials to more positive values,[21] but after addition of $LiClO_4$ there was still no reduction wave in the cyclic voltammogram of **1**.

Monomeric $[XZrW_5O_{18}]^{3-}$ Derivatives. The reactivity of the Zr−OMe bonds in **1** was exploited in the preparation of ^{17}O-enriched $[(X)ZrW_5O_{18}]^{3-}$ (X = OC_6H_5 **4**, OC_6H_4Me-4 **5**, OC_6H_4CHO-2 **6**, acac **7**, and OAc **8**) from ^{17}O-enriched $(^nBu_4N)_6$**1** and protic reagents HX. ^1H NMR showed that the reaction between approximately equimolar amounts of $(TBA)_6$**1** and *p*-cresol was only about 25% complete after heating to 80 °C for 1 h, which is consistent with the slow methanol

(16) Rocchiccioli-Deltcheff, C.; Thouvenot, R.; Dabbabi, M. *Spectrosc. Acta A* **1977**, *33*, 143.
(17) (a) Bradley, D. C.; Westlake, A. H. In *Proceedings of the Symposium on Coordination Chemistry*; Beck, M., Ed; Publishing House of the Hungarian Academy of Science: Budapest, 1965; pp 309−315. (b) Bradley, D. C.; Mehrotra, R. C.; Rothwell, I. P.; Singh, A. *Alkoxo and Aryloxo Derivatives of Metals*; Academic Press: London, 2001; pp 75−76.
(18) Day, V. W.; Klemperer, W. G.; Schwartz, C. *J. Am. Chem. Soc.* **1987**, *109*, 6030−6044.
(19) Boyer, M.; LeMeur, B. *C. R. Acad. Sci.* **1975**, *C281*, 59−62.
(20) (a) Zhang, J.; Bond, A. M.; MacFarlane, D. R.; Forsyth, S. A.; Pringle, J. M.; Mariotti, A. W. A.; Glowinski, A. F.; Wedd, A. G. *Inorg. Chem.* **2005**, *44*, 5123−5132. (b) Himeno, S.; Yoshihara, M.; Maekawa, M. *Inorg. Chim. Acta* **2000**, *298*, 165−171.
(21) Bond, A. M.; Vu, T.; Wedd, A. G. *J. Electroanal. Chem.* **2000**, *494*, 96−104.

Table 3. ^{183}W NMR Data

anion[a]	chemical shift/ppm[b] W_{ax}	W_{eq}
$[\{(\mu\text{-MeO})ZrW_5O_{18}\}_2]^{6-}$ **1**	64.4	37.6
$[\{(\mu\text{-HO})ZrW_5O_{18}\}_2]^{6-}$ **3**	68.0	40.4
$[(C_6H_5O)ZrW_5O_{18}]^{3-}$ **4**	45.2	32.6
$[(4\text{-MeC}_6H_4O)ZrW_5O_{18}]^{3-}$ **5**	39.4	27.7
$[\{2\text{-(CHO)C}_6H_4O\}ZrW_5O_{18}]^{3-}$ **6**	57.5	37.1
$[(OCMeCHCMeO)ZrW_5O_{18}]^{3-}$ **7**	63.8	38.8
$[(MeCO_2)ZrW_5O_{18}]^{3-}$ **8**	63.7	29.5
$[(Ph_2PO_2)ZrW_5O_{18}]^{3-}$ [c]	*d*	37.8

[a] All as tetrabutylammonium salts. [b] Positive values downfield of external 2 M aqueous Na_2WO_4 reference. [c] Proposed formula. [d] Not observed.

Table 4. ^{17}O NMR Data

anion[a]	chemical shift/ppm[b] W=O	ZrOW	WOW	W_6O	ZrOC
$[\{(\mu\text{-MeO})ZrW_5O_{18}\}_2]^{6-}$ **1**	711, 691	485	385, 377	−58	
$[\{(\mu\text{-MeO})(\mu\text{-HO})ZrW_5O_{18}\}_2]^{6-}$	*c*	482	*c*	−56	
$[\{(\mu\text{-HO})ZrW_5O_{18}\}_2]^{6-}$ **3**	712, 692	479	387, 378	−58	
$[(C_6H_5O)ZrW_5O_{18}]^{3-}$ **4**	725, 710	470	390, 384	−41	
$[(4\text{-MeC}_6H_4O)ZrW_5O_{18}]^{3-}$ **5**	722, 707	468	388, 382	−43	
$[\{2\text{-(CHO)C}_6H_4O\}ZrW_5O_{18}]^{3-}$ **6**	716, 699	481	388, 378	−57	
$[(OCMeCHCMeO)ZrW_5O_{18}]^{3-}$ **7**	714, 697	483	387, 377	−58	338
$[(MeCO_2)ZrW_5O_{18}]^{3-}$ **8**	720, 703	478	390, 380	−53	289
$[(Ph_2PO_2)ZrW_5O_{18}]^{3-}$ [d]	712, 693	491	387, 378	−60	

[a] All as tetrabutylammonium salts. [b] Positive values downfield of external water reference. [c] Not assigned. [d] Proposed formula.

exchange revealed by the EXSY study, so preparative reactions were heated at least overnight to ensure good conversions. Structures were determined by X-ray crystallography and are discussed in a following section.

^{183}W and ^{17}O NMR spectra of **4**−**8** (Tables 3 and 4) were consistent with heterometallic Lindqvist structures $[(X)ZrW_5O_{18}]^{3-}$, and ^1H NMR spectra contained the expected peaks for ligands X in addition to those for the TBA cations. The ^{183}W NMR data appear to show a correlation between the coordination number of zirconium in the anion and the chemical shift difference $\delta(W_{ax}) - \delta(W_{eq})$. For anions with seven-coordinate zirconium this difference lies in the range 20−34 ppm, whereas values for the two anions **4** and **5** with six-coordinate zirconium are 11.7 and 12.6 ppm. For $[(DMSO)_2(H_2O)(ZrW_5O_{18})]^{2-}$, which contains eight-coordinate zirconium, this difference is 33.8 ppm.[7]

In ^{17}O NMR spectra, terminal W=O and bridging WOW peaks for monomeric anions **4**−**8** were noticeably sharper than those for the dimeric anions **1** and **3**, with W_{eq}=O line widths ranging from 130 to 190 Hz for **4**−**8** compared with values of ca. 300 Hz for **1** and **3**. This is probably due to shorter correlation times for the smaller anions. Of particular interest in the ^{17}O NMR spectra of **7** and **8** were peaks at 338 and 289 ppm, respectively, in addition to those for the ZrW_5O_{18} oxide framework, which raises the possibility that the CO groups of acetylacetonate and acetate had been enriched in ^{17}O during the reactions between **1** and Hacac or HOAc. By comparison, resonances for the two nonequivalent acetylacetonate oxygens of $[Ti(O^iPr)_2(acac)_2]$ were observed in the natural abundance ^{17}O NMR spectrum at 324 and 353 ppm[22] and acetate resonances for $^nBu_3Sn(OAc)$ and $^nBu_2Sn(OAc)$ have been observed in the range 270−280 ppm in various solvents.[23] A possible mechanism for enrichment could involve exchange of ^{17}O in the ZrW_5O_{18} framework with traces of water in the reaction mixture, followed by reaction of the ^{17}O-enriched water with coordinated carbonyl groups resulting ultimately in C−O cleavage and transfer of ^{17}O to the ligand. We have demonstrated the exchange of framework oxygens with water, but we have yet to establish whether water reacts with the coordinated ligands in **7** and **8**.

Infrared spectra of the TBA salts of **4**−**8** show characteristic bathochromic shifts of terminal W=O vibrations due to the higher charge on $[(X)ZrW_5O_{18}]^{3-}$ anions compared with $[W_6O_{19}]^{2-}$, as well as vibrations associated with the ligands.

Attempts to prepare the diphenylphosphinate derivative $(TBA)_3[(Ph_2PO_2)ZrW_5O_{18}]$ from **1** and Ph_2PO_2H gave a crude product for which microanalysis results were close to this formulation. A peak at 17.9 ppm in the ^{31}P NMR spectrum is at lower frequency than those observed for bridging diphenylphosphinate in group 4 and 5 metal alkoxide complexes which have chemical shifts of ∼30 ppm.[24a] This suggests a monodentate bonding mode or a weakly associated diphenylphosphinate counterion by comparison with ^{31}P chemical shifts of 18.2 and 19.4 ppm for ion-paired $Ph_2PO_2^-$ in $[(^nBuSn)_{12}O_{14}(OH)_6](O_2PPh_2)_2$ and $[\{^nBuSn(OH)(O_2PPh_2)\}_3O](O_2PPh_2)$, respectively, and 31.0 ppm for the bridging diphenylphosphinates in the latter compound.[24b] The ^{17}O NMR spectrum was similar to those of $[\{(X)ZrW_5O_{18}\}_n]^{3n-}$ species with peaks for W=O at 712 and 693, ZrOW at 491, WOW at 387 and 378, and μ_6-O at −60 ppm. Additional peaks at higher frequencies in the W=O, ZrOW, and WOW regions showed that small amounts of other species were also present, the nature and implications of which are discussed later. The IR spectrum contained bands for ν(PO) at 1194 and 1127 cm^{-1}, ν(W=O) at 945 cm^{-1}, and several bands in the region 690−780 cm^{-1} due to overlapping bridging ν(W−O) and δ(CH) vibrations. Upon attempted recrystallization, a small number of crystals were obtained after several weeks, and an X-ray structure analysis revealed a protonated aggregate, $[(\mu_3\text{-HO})_2(ZrW_5O_{18})_3H]^{7-}$ **9** which contained no diphenylphosphinate. We have so far been unable to obtain suitable single crystals of $(TBA)_3[(Ph_2PO_2)ZrW_5O_{18}]$ for an X-ray crystal structure determination due to problematic oil formation in acetonitrile−ether mixtures, which may be related to the lability of the $Zr-O_2PPh_2$ bond.

Crystal Structures. Crystals suitable for X-ray crystal structure analysis were obtained by recrystallization from acetonitrile−ether. The nine structures reported here posed some very significant crystallographic challenges, with various combinations of large structure size, weak diffraction from small crystals, multiple occurrences of the chemical formula in the asymmetric unit, crystal twinning, pseudo-symmetry, and structural disorder of the principal anionic components, counterions, and solvent molecules. Several required the use of high-intensity synchrotron radiation for successful resolution. The main crystallographic data are summarized in Table 5, and full details of bond lengths and angles are given in the Supporting Information.

The crystal structure of **1** shown in Figure 8 revealed a dimeric anion with crystallographic inversion symmetry and

(22) Ridland, J. Ph.D. thesis, Newcastle University, 1998.

(23) Lycka, A.; Holecek, J. *Magn. Reson. Chem.* **2002**, *40*, 289−292.

(24) (a) Willett, K. Ph.D. thesis, Newcastle University, 2000. (b) Ribot, F.; Sanchez, C.; Willem, W.; Martins, J. C.; Biesemans, M. *Inorg. Chem.* **1998**, *37*, 911−917.

Table 5. Crystallographic Data

	(^{n}Bu$_4$N)$_6$**1**	(^{n}Bu$_4$N)$_6$**3**·MeCN	(^{n}Bu$_4$N)$_{12}$**3**·[W$_6$O$_{19}$][W$_{10}$O$_{32}$]	(^{n}Bu$_4$N)$_3$**4**	(^{n}Bu$_4$N)$_3$**5**
formula	$C_{98}H_{222}N_6O_{38}W_{10}Zr_2$	$C_{98}H_{221}N_7O_{38}W_{10}Zr_2$	$C_{192}H_{432}N_{12}O_{89}W_{26}Zr_2$	$C_{54}H_{113}N_3O_{19}W_5Zr$	$C_{55}H_{115}N_3O_{19}W_5Zr$
M_r	4113.8	4126.8	9298.1	2118.9	2133.0
crystal size (mm^3)	0.10 × 0.08 × 0.08	0.54 × 0.50 × 0.30	0.40 × 0.25 × 0.25	0.42 × 0.24 × 0.16	0.12 × 0.10 × 0.02
temperature, K	150	150	160	160	150
crystal system	monoclinic	monoclinic	triclinic	monoclinic	orthorhombic
space group	*I*2/*a*	*C*2/*c*	$P\bar{1}$	$P2_1/n$	*Pnma*
a, Å	24.367(5)	42.705(9)	17.5165(6)	16.2557(7)	23.8193(11)
b, Å	15.987(3)	16.063(4)	17.6777(6)	23.8817(11)	17.1071(8)
c, Å	35.379(8)	24.531(10)	24.2402(9)	18.4678(8)	17.2814(8)
α, deg			74.861(2)		
β, deg	91.155(4)	123.664(14)	70.185(2)	90.018(2)	90
γ, deg			79.242(2)		
V, Å^3	13 779(5)	14 006(7)	6776.6(4)	7169.5(5)	7041.8(6)
Z	4	4	1	4	4
D_{calcd}, g cm^{-3}	1.983	1.959	2.278	1.963	2.012
λ, Å	0.6900	0.710 73	0.710 73	0.710 73	0.6934
μ, mm^{-1}	8.52	8.39	11.13	8.19	8.34
θ_{max}, deg	25.0	25.0	25.0	28.9	22.7
reflections measured	11 662	48 162	48 534	45 173	34 974
unique reflections	11 662	11 842	23 595	16 952	5245
R_{int} (on F^2)	0	0.080	0.043	0.047	0.087
no. of parameters	541	722	1478	782	416
R^a [$F^2 > 2\sigma(F^2)$]	0.087	0.054	0.043	0.041	0.100
$R_w{}^b$ (all data)	0.288	0.162	0.103	0.101	0.218
GOF^c (*S*)	1.24	1.12	1.03	0.98	1.34
max, min diff map, e Å^{-3}	6.98, −3.05	2.19, −2.28	5.82, −4.92	1.69, −1.53	3.02, −5.02

	(^{n}Bu$_4$N)$_3$**6**·0.5MeCN	(^{n}Bu$_4$N)$_3$**7**·0.5Et$_2$O	(^{n}Bu$_4$N)$_3$**8**	(^{n}Bu$_4$N)$_7$**9**·3.5MeCN
formula	$C_{56}H_{114.5}N_{3.5}O_{20}W_5Zr$	$C_{57}H_{125}N_3O_{21}W_5Zr$	$C_{50}H_{111}N_3O_{20}W_5Zr$	$C_{119}H_{265.5}N_{10.5}O_{56}W_{15}Zr_3$
M_r	2167.5	2199.1	2084.9	5771.3
crystal size (mm^3)	0.15 × 0.15 × 0.10	0.40 × 0.36 × 0.30	1.00 × 0.40 × 0.05	0.10 × 0.06 × 0.02
temperature, K	150	160	160	150
crystal system	orthorhombic	monoclinic	monoclinic	monoclinic
space group	*Pbcn*	$P2_1$	$P2_1/n$	*C*2
a, Å	24.7085(9)	16.9153(7)	15.857(3)	66.456(6)
b, Å	36.0065(12)	24.9724(10)	23.723(5)	15.6607(14)
c, Å	33.1734(11)	17.9490(7)	18.663(4)	32.988(3)
α, deg				
β, deg	90	90.054(2)	90.33(3)	93.722(2)
γ, deg				
V, Å^3	29 513.3(18)	7581.9(5)	7020(2)	34260(5)
Z	16	4	4	8
D_{calcd}, g cm^{-3}	1.511	1.926	1.973	2.238
λ, Å	0.6900	0.710 73	0.710 73	0.6900
μ, mm^{-1}	7.96	7.75	8.37	10.27
θ_{max}, deg	25.0	28.4	22.5	24.2
reflections measured	226 421	65 021	40 689	80 097
unique reflections	28 403	34 101	9172	43 160
R_{int} (on F^2)	0.063	0.039	0.041	0.046
no. of parameters	1726	1539	788	3665
R^a [$F^2 > 2\sigma(F^2)$]	0.052	0.035	0.035	0.052
$R_w{}^b$ (all data)	0.127	0.068	0.085	0.122
GOF^c (*S*)	1.28	1.02	1.06	1.03
max, min diff map, e Å^{-3}	1.97, −2.56	1.31, −1.64	1.69, −1.46	2.91, −1.69

^{a} $R = \sum||F_o| - |F_c||/\sum|F_o|$. ^{b} $R_w = [\sum w(F_o^2 - F_c^2)^2/\sum w(F_o^2)^2]^{1/2}$. ^{c} GOF = $[\sum w(F_o^2 - F_c^2)^2/(\text{no. of unique reflns} - \text{no. of params})]^{1/2}$.

seven-coordinate Zr bonded symmetrically to bridging methoxide groups (for which the H atoms were not located). The Zr−O(C) bond lengths of 2.182(15) Å and O1ZrO1 and ZrO1Zr angles of 68.1(7)° and 111.9(7)° are the same as those in the structure of [{(η^5-C$_5$Me$_5$)Zr(OMe)$_2$(μ-OMe)}$_2$],[25] and the bridging oxygen O1 is trigonal planar, the sum of angles being 360°. Klemperer has shown that the alkylated bridging oxygen in [(μ-MeO)Nb$_2$W$_4$O$_{18}$]$^{3-}$ is pyramidal,[18] so the trigonal methoxide in **1** is likely to be due to the steric constraints imposed by the two ZrW$_5$O$_{18}$ units. The two ZrW$_5$O$_{18}$ oxide fragments are eclipsed, with O$_c$−Zr−Zr−O$_c$′ torsion angles of 1.7° and 3.0 ° and an O$_c$···O$_c$′ distance of 4.83 Å between opposite ZrW$_3$ planes. The Zr(μ-OMe)$_2$Zr plane bisects the largest O$_c$ZrO$_c$ angles and occupies the mean position between the two ZrW$_3$ planes. The dimeric structure of **1** contrasts with the mononuclear titanium analogue **2**[5] and can be rationalized in terms of the tendency of the larger Zr to adopt coordination numbers greater than six.

The structure of **3** is shown in Figure 9 and is similar to that of **1** in that the two ZrW$_5$ units are eclipsed, with angles between opposite ZrW$_3$ planes of 0.2° and 1.3°, but a significant

(25) Heyn, R. H.; Stephan, D. W. *Inorg. Chem.* **1995**, *34*, 2804−2812.

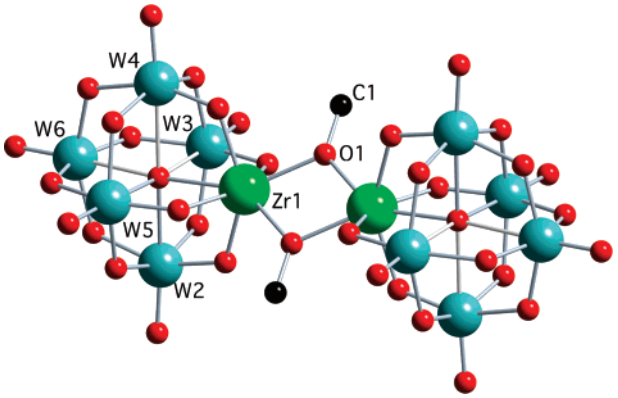

Figure 8. Diagram of the $[\{(\mu\text{-MeO})ZrW_5O_{18}\}_2]^{6-}$ anion **1**.

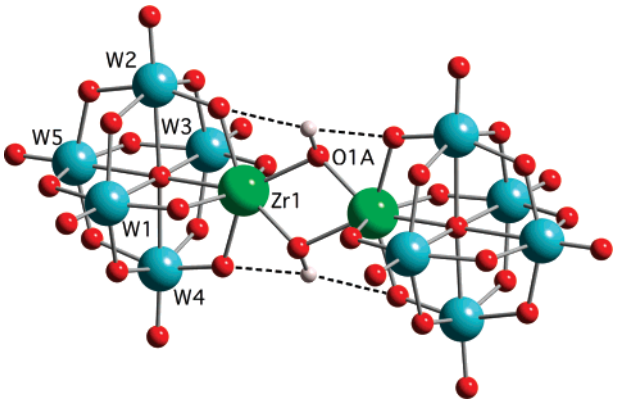

Figure 9. Diagram of the $[\{(\mu\text{-HO})ZrW_5O_{18}\}_2]^{6-}$ anion **3**. Hydrogen atoms, not located crystallographically, have been added to show possible hydrogen bonding interactions in the bridging region.

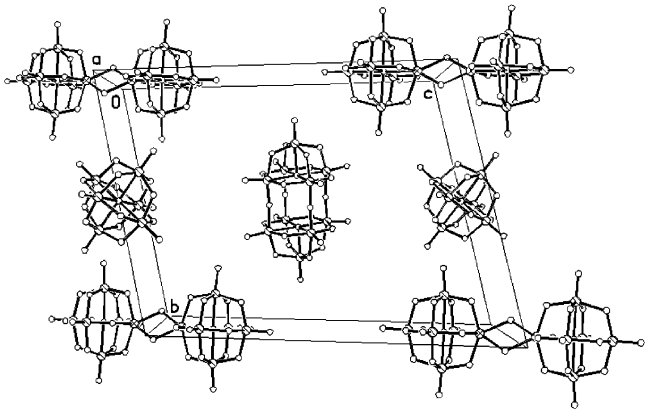

Figure 10. Diagram showing the anion packing in $(TBA)_{12}$**3**·$[W_6O_{19}]$-$[W_{10}O_{32}]$.

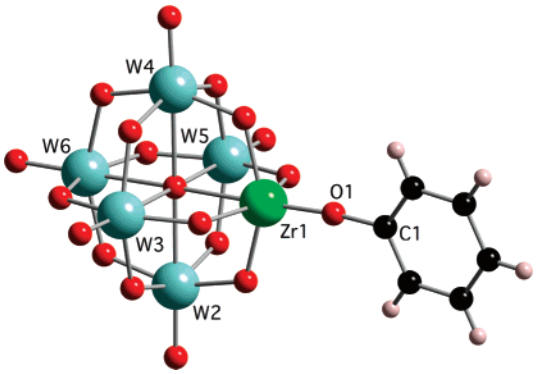

Figure 11. Diagram of the major anion component $[(C_6H_6O)ZrW_5O_{18}]^{3-}$ in the structure of $(TBA)_3$**4**.

difference is that the $Zr(\mu\text{-OH})_2Zr$ plane is disordered between two orientations, each of which is offset toward a set of four O_c atoms such that the angles between the bridging plane and the two orthogonal ZrW_3 planes are 24.4° and 66.6°, i.e., a rotation of 21° from the mean position. Although the hydrogen of the OH group was not detected in the X-ray structure, by setting the O−H bond length to 0.95 Å the orientation of the $Zr(\mu\text{-OH})_2Zr$ plane can be seen to optimize $O_c\cdot\cdot H\cdot\cdot O_c$ hydrogen bonding when O1 is pyramidal and the sum of the angles is 333°, only 5° greater than the tetrahedral value. The structure of **3** is similar to that in the hydrate $(TBA)_6$**3**·$2H_2O$ reported by Villanneau, in which the bridging plane is also rotated from the mean position, but in this case by 15°. A similar arrangement of hydrogen bonding can therefore be envisaged for the hydrated compound which, with an O−H bond length of 0.95 Å, requires a pyramidal bridging oxygen where the sum of angles is about 320°.

Figure 10 shows a partial packing diagram for the cocrystal $(TBA)_{12}$**3**·$[W_6O_{19}][W_{10}O_{32}]$ which was unexpectedly obtained from the product of prolonged hydrolysis of **1**. To our knowledge, this is the first example of cocrystallization of three different polyoxometalates. Bond lengths and angles for the $[W_6O_{19}]^{2-}$ and $[W_{10}O_{32}]^{4-}$ anions are similar to those previously observed,[26,27] and the structure of **3** within this cocrystal is essentially the same as that in $(TBA)_6$**3** described above, although in this case the $Zr(\mu\text{-OH})_2Zr$ plane is rotated by 16° from the mean position between the two ZrW3 planes.

In contrast to the methoxide **1** and hydroxide **3**, the aryloxide derivatives $[(4\text{-}RC_6H_4O)ZrW_5O_{18}]^{3-}$ (R = H, **4**; R = Me, **5**) are monomeric with terminal aryloxide ligands and six-coordinate zirconium. Although not shown in Figure 11, the Zr—OPh and W═O groups in the phenoxide **4** are disordered over two mutually *trans* sites. The plane of the phenoxide ligand in the major component (shown) is almost aligned with one of the ZrW_3 planes (OZrC1C3 pseudo-torsion angle *ca.* 7°) with a Zr−O bond length of 1.866(6) Å and a ZrOC angle of 175.0-(8)°, whereas the aryloxide in the minor component is oriented between the two ZrW_3 planes (pseudo-torsion angles near 45°) with Zr—O 1.808(6) Å and ZrOC 175.9(8)°. The end-to-end disorder is not present in the structure of **5**, and the aryloxide in this case lies on a mirror plane which bisects the angle between the two ZrW_3 planes as shown in Figure 12, with a Zr—O bond length of 2.03(3) Å and a ZrOC angle of 142(3)°. Shorter M—O bonds in group 4 aryloxide compounds have been ascribed to oxygen-p to metal-d π-bonding,[28] but the short Zr—O bond in **4** may be partly due to the disorder involving the W═O bond and, in addition, the estimated uncertainty in the Zr—O bond length in **5** is fairly large. Similarly, uncertainties in C—O bond lengths are too large for any meaningful comparison. Studies of early transition metal aryloxides have shown that the ZrOC bond angle is an unreliable indicator of

(26) Fuchs, J.; Freiwald, W.; Hartl, H. *Acta Crystallogr., Sect. B* **1978**, *34*, 1764−1770.
(27) Fuchs, J.; Hartl, H.; Schiller, W.; Gerlach, U. *Acta Crystallogr., Sect. B* **1976**, *32*, 740−749.
(28) Bradley, D. C.; Mehrotra, R. C.; Rothwell, I. P.; Singh, A. *Alkoxo and Aryloxo Derivatives of Metals*; Academic Press: London, 2001; p 467.

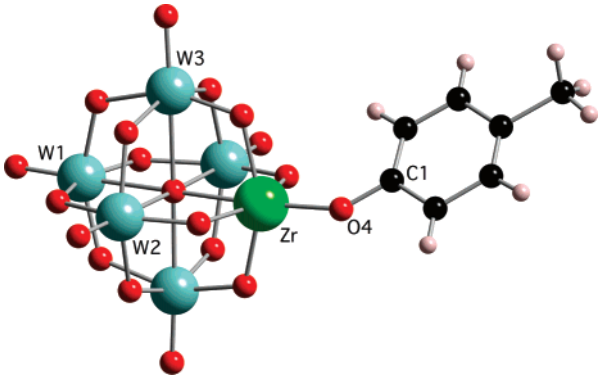

Figure 12. Diagram of the $[(4\text{-}MeC_6H_4O)ZrW_5O_{18}]^{3-}$ anion **5**.

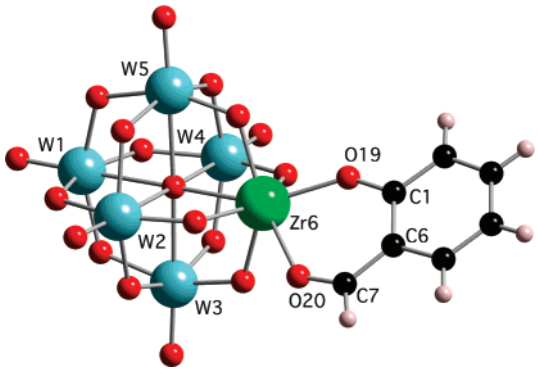

Figure 13. Diagram of the $[\{2\text{-}(CHO)C_6H_4O\}ZrW_5O_{18}]^{3-}$ anion **6**.

oxygen-to-metal π-bonding,[29] and it is not possible to draw any firm conclusions about the comparative Zr—OAr bonding in **4** and **5** from these structures.

While zirconium in the monomeric aryloxides **4** and **5** remains six-coordinate, the salicylaldehyde ligand in **6** is able to bind in a chelating fashion to give seven-coordinate zirconium, and of the two crystallographically independent anions in the crystal structure of **6**, the one without disorder is shown in Figure 13. The plane of the salicylaldehyde bisects the angle between the two ZrW_3 planes, and the Zr—O19 bond distance of 2.095(7) Å is the same as the Zr—O bond in **5** within experimental error which, together with the Zr—O(20) bond length of 2.331(8) Å, indicates an asymmetric "aryloxide and aldehyde" bonding mode for salicylaldehyde in **6**, with a OZrO bite angle of 73.5(3)°. This is consistent with a previously characterized zirconium salicylaldehyde complex.[30]

Zirconium is also seven-coordinate in acetylacetonate **7** (Figure 14) and acetate **8** (Figure 15). The acetylacetonate is symmetrically bound, with Zr—O bond lengths of 2.187(8) and 2.224(9) Å and C—O bond lengths of 1.265(13) and 1.269(15) Å. The OZrO bite angle is 74.2(3)°, and the plane through O61A, Zr6A, and O62A bisects the angle between the two ZrW_3 planes (the plane of the ligand is tilted slightly off the longitudinal W—O—Zr axis by about 4°). In **8** there is some disorder between Zr(OAc) and the *trans*-W═O group, although the Zr—O bond lengths of 2.373(11) and 2.345(11) Å, C—O bond lengths of 1.28(2) and 1.24(2) Å, and bite angle of 54.3-

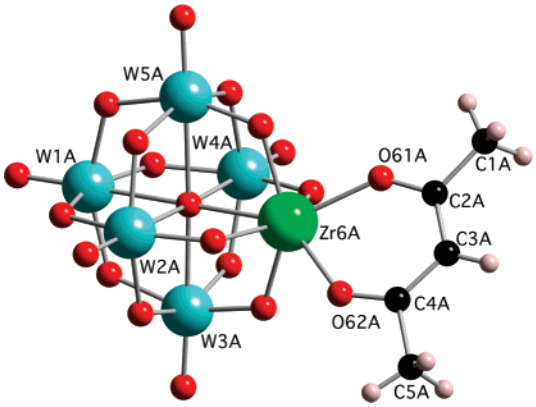

Figure 14. Diagram of the $[(acac)ZrW_5O_{18}]^{3-}$ anion **7**.

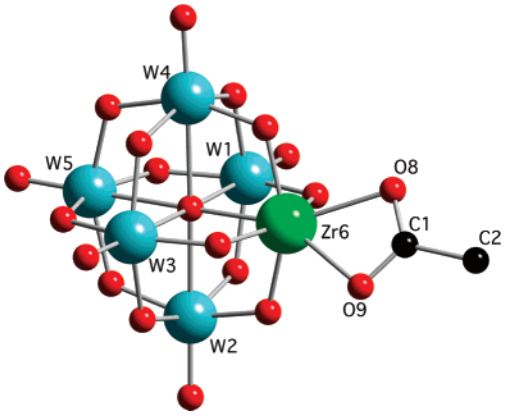

Figure 15. Diagram of the $[(CH_3CO_2)ZrW_5O_{18}]^{3-}$ anion **8**.

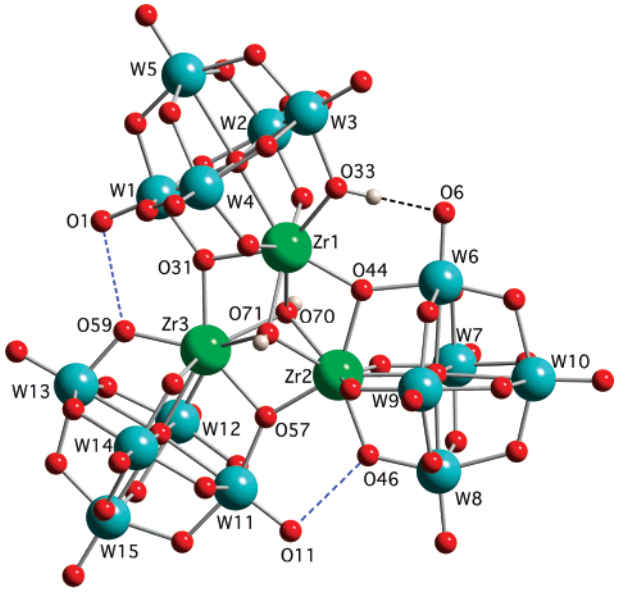

Figure 16. Diagram of the anion $[(\mu\text{-}OH)_2(ZrW_5O_{18})_3H]^{7-}$ **9**.

(4)° for the acetate ligand are similar to those for the chelating acetate in $[(\eta^5\text{-}C_5Me_5)_2Zr(OAc)_2]$.[31]

The structure of **9** is shown in Figure 16 and can be seen to be an aggregate of three ZrW_5O_{18} units linked through two μ_3-OH groups and by bonds between one ZrOW bridging oxygen of each unit and the zirconium of an adjacent unit so that each zirconium is eight-coordinate. The formula from the X-ray

(29) Smith, G. D.; Fanwick, P. E.; Rothwell, I. P. *Inorg. Chem.* **1990**, *29*, 3221—3226.
(30) Matilainen, L.; Klinga, M.; Leskela, M. *J. Chem. Soc., Dalton Trans.* **1996**, 219—225.
(31) Howard, W. A.; Trnka, T. M.; Waters, M.; Parkin, G. *J. Organomet. Chem.* **1997**, *528*, 95—121.

crystal structure determination required three protons for charge balance, and although these were not located, bond valence sum calculations[32] enabled us to identify the protonated sites as the two triply bridging oxygens O70 and O71 and one of the ZrOW bridging oxygens O33. BVS sums for O70 and O71 are 1.14 and 1.26, respectively, and for the ZrOW oxygens O33, O46, and O59 BVS sums are 1.29, 1.95, and 2.02, respectively. Figure 16 shows that a hydrogen on O33 with an O−H bond distance of 0.95 Å is able to hydrogen bond to the terminal oxygen O6 with an O···O distance of 2.765 Å, while the distances between O46 and O11 and between O59 and O1 of 2.767 and 2.785 Å, respectively, suggest that these are also potential protonation sites (corresponding distances in the other anion of the asymmetric unit are 2.648, 2.825, and 2.800 Å, respectively). Protonation of O33 causes elongation of the associated W−O and Zr−O bonds as predicted by DFT calculations on zirconium-substituted Keggin structures.[4g] Figure 16 also shows that the hydrogen of each μ_3-OH group sits within a pocket formed by three ZrOW oxygens which may also serve to stabilize protons at these sites. The structure of **9** can also be regarded as an assembly of three $\{W_5O_{18}\}^{6-}$ units around a $\{Zr_3(\mu\text{-OH})_2\}^{10+}$ core, and a similar motif has been observed in the aggregate $[Zr_6O_2(OH)_4(H_2O)_3(\beta\text{-SiW}_{10}O_{37})_3]^{14-}$ in which three $\{ZrSiW_{10}O_{37}\}$ units are arranged in an asymmetric fashion around the Zr_3 core.[4f]

In all of these ZrW_5 structures, $W_{eq}-O_c$ bonds are shorter than $W_{eq}-O_d$ bonds (except where O_c is protonated or bonded to another zirconium as in **9**) reflecting an asymmetric electron distribution in the W−O−Zr bonding, possibly with a larger ionic contribution to Zr−O bonds, and lending support to the view of these anions as zirconium complexes of the lacunary oxometalate ligand $\{W_5O_{18}\}^{6-}$.

3. Discussion

The high-yield, selective synthesis of zirconotungstate **1** by hydrolysis of a mixture of a zirconium alkoxide and $[\{WO(OMe)_4\}_2]$ in the presence of WO_4^{2-} is remarkable. A range of polynuclear products from metal alkoxide hydrolysis has been characterized,[28,33] and several have been used as building blocks in the preparation of hybrid organic−inorganic materials,[34] but the reactions involved in their formation are poorly understood. What is more, incommensurate hydrolysis rates in mixtures of metal alkoxides are likely to result in complex mixtures of products, making it difficult to predict or control with any certainty the ultimate products from such reactions. Hence, in the sol−gel production of mixed oxides from alkoxides, some control over stoichiometry and aggregation is generally achieved by the addition of "modifier" ligands, often on an empirical basis.[35] Although we currently know little about aggregation mechanism or the nature of intermediates in the nonaqueous hydrolytic synthesis of **1**, we have previously demonstrated that facile ligand redistribution occurs in the reaction between WO_4^{2-} and $WO(OMe)_4$ to give $[W_2O_5(OMe)_4]^{2-}$.[36] ZrW_5 Lindqvist structures clearly represent an energy minimum in the landscape of possible hydrolysis products from the reaction shown in Scheme 1, and putative intermediates $[Zr_xW_yO_p(OH)_q(OR)_r]^{n-}$ must rearrange readily for high yields of **1** to be obtained.

The coordination number of zirconium in the $[\{(X)ZrW_5O_{18}\}_n]^{3n-}$ polyoxometalates described here appears to be determined by steric interactions between the ligand X and the oxide cage, and space-filling representations of **1**, **3**, **5**, **6**, and **7** are shown in Figure 17. It is apparent that, for monodentate ligands that are not substituted at the atom which is β to Zr, seven-coordination can be achieved by dimerization, as in the

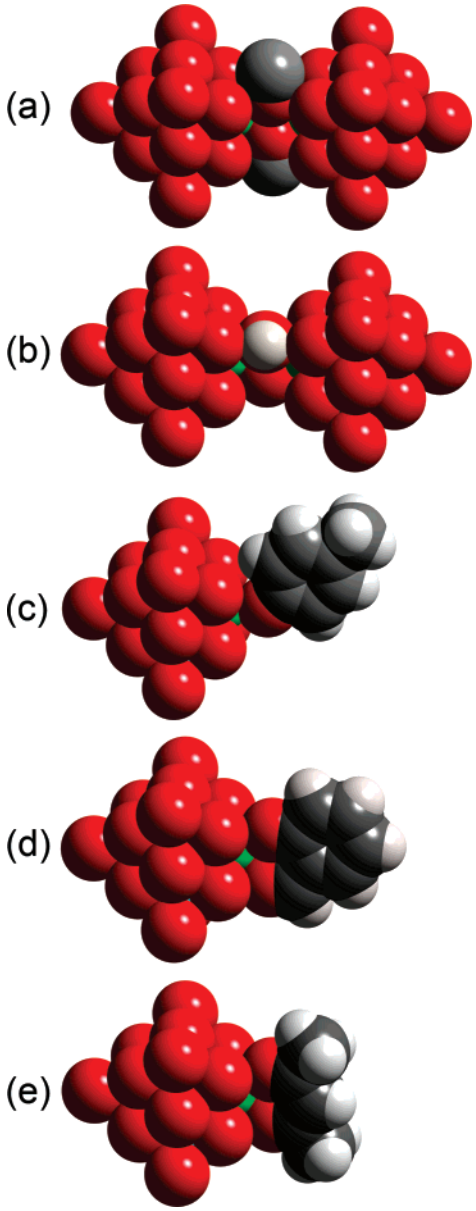

Figure 17. Space-filling representations of anions **1** (a), **3** (b), **5** (c), **6** (d), and **7** (e).

(32) Brown, I. D.; Altermatt, D. *Acta Crystallogr., Sect. B* **1985**, *41*, 244−247.
(33) (a) Watenpaugh, K.; Caughlan, C. N. *Chem. Commun*. **1967**, 76−77. (b) Morosin, B. *Acta Crystallogr., Sect. B* **1977**, *33*, 303−305. (c) Schmid, R.; Mosset, A.; Galy, J. *J. Chem. Soc., Dalton Trans.* **1991**, 1999−2005. (d) Day, V. W.; Eberspacher, T. A.; Klemperer, W. G.; Park, C. W.; Rosenberg, F. S. *J. Am. Chem. Soc.* **1991**, *113*, 8190−8192. (e) Day, V. W.; Eberspacher, T. A.; Klemperer, W. G.; Park, C. W. *J. Am. Chem. Soc.* **1993**, *115*, 8469−8470. (f) Day, V. W.; Eberspacher, T. A.; Chen, Y.; Hao, J.; Klemperer, W. G. *Inorg. Chim. Acta* **1995**, *229*, 391−405. (g) Campana, C. F.; Chen, Y.; Day, V. W.; Klemperer, W. G.; Sparks, R. A. *J. Chem. Soc., Dalton Trans.* **1996**, 691−702. (h) Day, V. W.; Klemperer, W. G.; Pafford, M. M. *Inorg. Chem.* **2005**, 5397−5404. (i) Fornasieri, G.; Rozes, L.; Le Calvé, S.; Alonso, B.; Massiot, D.; Regre, M. N.; Evain, M.; Boubekeur, K.; Sanchez, C. *J. Am. Chem. Soc.* **2005**, *127*, 4869−4878.
(34) Sanchez, C.; Soler-Illia, G. J. A. A.; Ribot, : Lalot, T.; Mayer, C. R.; Cabuil, V. *Chem. Mater*. **2001**, *13*, 3061−3083.
(35) Schubert, U. *J. Mater. Chem.* **2005**, *15*, 3701−3715.
(36) Clegg, W.; Errington, R. J.; Fraser, K. A.; Richards, D. G. *Chem. Commun.* **1993**, 1105−1107.

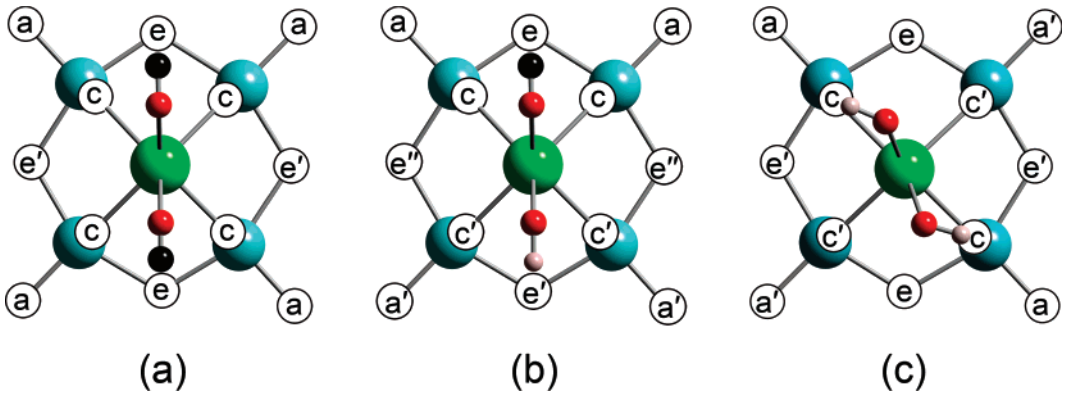

Figure 18. Views along Zr−Zr vectors onto (a) (μ-MeO)$_2$ZrW$_5$ unit of **1**, (b) (μ-MeO)(μ-HO)$_2$ZrW$_5$ unit of [(MeO)(HO)(ZrW$_5$O$_{18}$)$_2$]$^{6-}$, and (c) (μ-HO)$_2$-ZrW$_5$ unit of **3**.

methoxide **1** and the hydroxide **3**. The Zr(μ-OMe)$_2$Zr plane in **1** is oriented so as to minimize steric interactions between the methoxide groups and the oxide cage, while the orientation of the rotated Zr(μ-OH)$_2$Zr bridging plane in **3** can be explained by hydrogen bonding between OH and the ZrOW oxygens, shown in Figure 17b. For the monomeric aryloxides **4** and **5**, a reduction in the ZrOC angle necessary to enable the aryloxide to become bridging (the ZrOC angle in **1** is 123° whereas that in **5** is 142°) would introduce unfavorable interactions between the *ortho* positions of the aryloxide and ZrOW oxygens, while Figure 17d and e show clearly that there is no steric hindrance to chelation in **6** and **7**. The close approach of an alkyl group to the oxide surface may facilitate hydrogen abstraction and loss of alkene, i.e., the reverse of alkene activation on an acidic oxide surface, and we are now investigating the reactivity of anions [(RO)ZrW$_5$O$_{18}$]$^{3-}$ with more ramified alkoxide groups.

Our NMR studies of **1** and **3** raise some interesting questions regarding solution dynamics and substitution mechanisms. Variable-temperature ^{1}H NMR spectra of **1** did not show any evidence of a dimer−monomer equilibrium in solution, but if the dimeric structure is retained in solution, two W$_{eq}$OW$_{eq}$ peaks for e and e′ in Figure 18a should be observed in addition to a peak for W$_{eq}$OW$_{ax}$, i.e., a total of three peaks in the WOW region of the ^{17}O NMR spectrum. In fact, only two WOW peaks are observed as shown in Figure 1, but the broader nature of the upfield peak may be the result of e/e′ site exchange through a process equivalent to rotation of the bridging plane relative to the ZrW$_5$ units. The asymmetry in **3** should also be reflected in the W=O and WOW regions of the ^{17}O NMR spectrum, as shown for the inequivalent a, a′ and e, e′ sites in Figure 18c, and again, the broader lines observed for peaks in these regions may be the result of site exchange in addition to correlation times. Further evidence for dynamic behavior in these dimers comes from the relatively sharp single ZrOW peaks in ^{17}O NMR spectra for **3** and the proposed hydrolysis intermediate [(MeO)(HO)(ZrW$_5$O$_{18}$)$_2$]$^{6-}$, whereas two peaks labeled c and c′ in Figure 18b and c would be expected.

Protonolysis of **1** with HX provides convenient access to a wide range of derivatives as shown in Scheme 1, but mechanistic details of these reactions are largely unknown. The slow rate of methanol exchange with **1**, as shown by 2D ^{1}H EXSY NMR, and the relatively slow reactions with *p*-cresol and water emphasize the stability of the dimeric structure and could imply the initial dissociation of the dimer prior to coordination of HX with subsequent proton transfer and loss of MeOH (mechanism

Scheme 2. Possible Mechanisms for Reactions with HX at the Zirconium Site in **1**

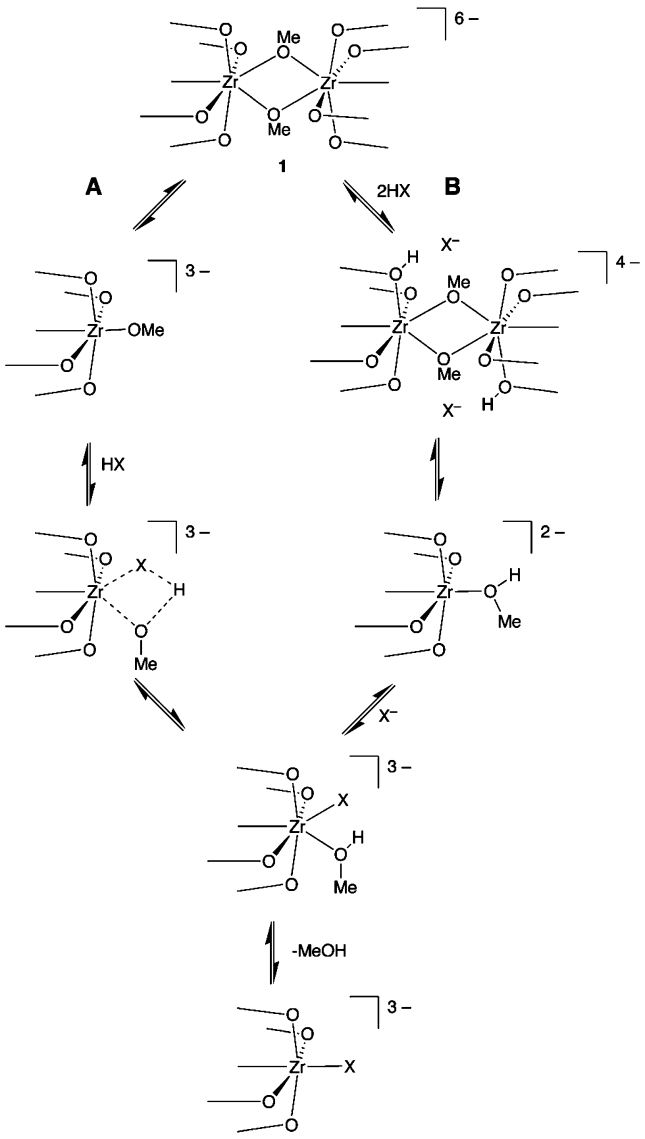

A in Scheme 2). Given the comparatively high charges on the ZrW$_5$ units and the associated basicity of ZrOW oxygen sites,[37] it is perhaps more likely that protonation of the surface oxygens

(37) Fernández, J. A; López, X.; Poblet, J. M. *J. Mol. Catal. A: Chem.* **2007**, *262*, 236−242.

of the POM occurs first, probably at the ZrOW sites, with subsequent proton migration to methoxide resulting in bridge cleavage, followed by coordination of X^- and dissociation of MeOH (mechanism **B** in Scheme 2).

Dimer dissociation in Scheme 2 is likely to be promoted in good donor solvents to give monomeric species $[L_2(MeO)ZrW_5O_{18}]^{3-}$ *via* **A** or $[L_2(MeOH)ZrW_5O_{18}]^{2-}$ *via* **B**, and peaks associated with solvated monomeric dianions were present in the ESI mass spectra of **1** and **3**. Water exchange in $[(DMSO)_n(H_2O)_{3-n}ZrW_5O_{18}]^{2-}$ ($n = 0, 1$) has been shown to be very slow, but upon addition of the stronger nucleophile OH^- to $[(H_2O)_3ZrW_5O_{18}]^{2-}$ the dimer **3** was formed[7,8] presumably *via* $[(H_2O)_2(HO)ZrW_5O_{18}]^{3-}$. The higher charge on this intermediate would be expected to increase the lability of the water, which must be lost in the formation of **3**. The broad peak observed at 177 ppm in the ^{17}O NMR study of oxygen exchange in **3** may therefore be due to coordinated water in species resulting from either partial or complete dissociation of **3**.

^{17}O exchange in these anions is expected to proceed *via* proton transfer and involves all framework oxygens to different degrees, although the ZrOW oxygens appear to be the most enriched and, hence, most labile. Studies of oxygen exchange between hexaniobates $[H_xNb_6O_{19}]^{(8-x)-}$ and water showed no evidence for intramolecular ^{17}O exchange between the different terminal and bridging sites, and to explain the pH-dependent exchange rates with bulk water, it was proposed that Nb−(μ_2-O)−Nb bonds in any one of the three Nb_4 planar rings undergo concerted cleavage to generate a metastable form of the anion containing five-coordinate niobium to which incoming water can bind prior to proton transfer and oxygen exchange.[38] A similar process in **3** would require cleavage of W−(μ_2-O) bonds in the axial ZrW_3 and equatorial W_4 planar rings, which are likely to have different energetic requirements, resulting in different rates of exchange for O_e compared with O_d. The approximate amounts of enrichment at the different sites after 2 weeks, taken from the spectrum in Figure 5d, increase in the order $O_f < O_d \approx O_e < O_b < O_a < O_c$, although at early stages one of the WOW sites $O_{d/e}$ appears to be enriched more rapidly as shown in Figure 5b and c.

Most of our work demonstrates that the ZrW_5O_{18} unit is fairly robust, but the observation of $[W_{10}O_{32}]^{4-}$ and $[W_6O_{19}]^{2-}$ in samples of **1** and **3** that were exposed to water, particularly at elevated temperatures, suggests that the oxide framework is sufficiently labile to lose zirconium under appropriate conditions. Although the $W_5O_{18}^{6-}$ fragment is not normally regarded as a stable species, Pope has demonstrated its kinetic stability in aqueous reactions involving the dissociation of $[Ce\{W_5O_{18}\}_2]^{8-}$,[39] so it seems plausible that W_5 fragments generated from **1** or **3** could assemble to give $[W_{10}O_{32}]^{4-}$, which has in turn been shown to interconvert with $[W_6O_{19}]^{2-}$ in organic solvents.[19] This factor must therefore be borne in mind when studying the reactivity of this heterometalate.

The isolation of **9** from the reaction between **1** and Ph_2PO_2H demonstrates that aggregation beyond the hydroxide dimer **3** is possible and suggests that the $Zr-O_2PPh_2$ bond is more labile than Zr−OAc, probably because the chelating mode for $Ph_2PO_2^-$ is more strained than that for OAc^-. With this in mind,

Scheme 3. Formation of **9** in the Reaction between **1** and Ph_2PO_2H

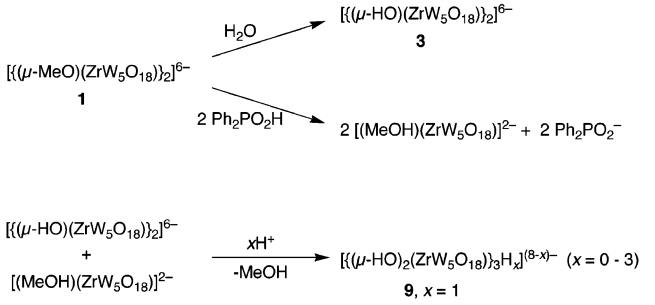

the structure of **9** can be viewed as an aggregate of **3** with $[L_nZrW_5O_{18}]^{2-}$, where the latter anion could be formed either by dissociation of $Ph_2PO_2^-$ from $[(Ph_2PO_2)ZrW_5O_{18}]^{3-}$ or by protonation and dissociation of dimer **1**, as shown in Scheme 3 with Ph_2PO_2H acting as an acid of a noncoordinating anion. The resulting aggregate $[(\mu\text{-HO})_2(ZrW_5O_{18})_3]^{8-}$, when protonated at the ZrOW sites indicated in Figure 16, would give anions $[(\mu\text{-HO})_2(ZrW_5O_{18})_3H_x]^{(8-x)-}$ ($x = 1 - 3$) of which **9** is the anion with $x = 1$.

This implies that the rational assembly of ZrW_5O_{18} building blocks into larger aggregates should be possible, and preliminary results confirm that protonation of **1** with 2 mol equiv of aqueous HBF_4 produces species of the type $[L_nZrW_5O_{18}]^{2-}$, as shown by the strong $\nu(W{=}O)$ band at 961 cm^{-1}, compared to 962−964 cm^{-1} reported for DMSO and aqua derivatives,[7] and by peaks in the ^{17}O NMR spectrum that are shifted significantly to higher frequencies compared with those observed for the more highly charged $[XZrW_5O_{18}]^{3-}$ oxometalates (Figures S11 and S12 in Supporting Information). What is more, the ^{17}O NMR peaks for the $[L_nZrW_5O_{18}]^{2-}$ species so generated coincide with the impurity peaks in the ^{17}O NMR spectrum of crude $[(Ph_2PO_2)ZrW_5O_{18}]^3$, providing evidence that the diphenylphosphinate does indeed dissociate in solution. When the amount of HBF_4 added to **1** was reduced to that required to form **9** (1.3 mol equiv), the ^{17}O NMR spectrum of the product contained several peaks in the ZrOW region and three peaks in the μ_6-O region, as would be expected for an asymmetric aggregate such as **9** (Figure S13 in Supporting Information).

The serendipitous isolation of $(TBA)_7$**9** was therefore fortuitous in that it alerted us to solution dynamics and aggregation processes involved in the formation of high nuclearity polyoxometalate structures. Further studies of the formation of **9** and related structures and of protonation reactions with other acids of weakly coordinating anions will be described separately.

4. Summary

We have developed a reliable nonaqueous hydrolytic methodology for the synthesis of the alkoxide-functionalized zirconium pentatungstate $[\{(\mu\text{-MeO})ZrW_5O_{18}\}_2]$ **1** which enables efficient preparation of ^{17}O-enriched samples for NMR studies and provides access to a broad range of metalorganic derivatives through systematic ligand exchange. Structural studies have highlighted the importance of steric effects at the surface of the ZrW_5O_{18} oxide framework and the consequences of protonation at ZrOZr and ZrOW bridging oxygens. Methanol exchange and hydrolysis were slower than might have been

(38) Black, J. R.; Nyman, M.; Casey, W. H. *J. Am. Chem. Soc.* **2006**, *128*, 14712−14720.
(39) Belai, N.; Sadakane, M.; Pope, M. T. *J. Am. Chem. Soc.* **2001**, *123*, 2087−2088.

expected, and our NMR studies revealed an intermediate, [(μ-HO)(μ-MeO)(ZrW_5O_{18})$_2$]$^{6-}$, in the formation of [{(μ-HO)-ZrW_5O_{18}}$_2$] **3**, which is reversible. While mononuclear species [(X)ZrW_5O_{18}]$^{3-}$ with either six-coordinate (X = OC_6H_5 **4**, OC_6H_4Me-4 **5**) or seven-coordinate zirconium (X = OC_6H_4-(CHO)-2 **6**, acac **7**, OAc **8**) were formed in reactions with HX, higher aggregation was observed when the anion was more weakly bound to {ZrW_5O_{18}}$^{2-}$, as in the reaction between **1** and Ph_2PO_2H which led to the isolation of the protonated aggregate [(μ_3-HO)$_2$(ZrW_5O_{18})$_3$H]$^{7-}$ **9**. Although we have yet to determine the relative acidities of the various surface protons in **3** and **9**, this may provide an insight into the nature of acid sites generated with the polynuclear species that have been proposed on the surface of tungstated zirconia catalysts.

5. Experimental Section

General. All reactions and manipulations were carried out under dry, oxygen-free nitrogen using Schlenk techniques or in a drybox fitted with a recirculation system.[40] Hydrocarbon and ether solvents were dried over and distilled from sodium-benzophenone, acetonitrile was dried over and distilled from calcium hydride, and methanol was distilled from magnesium methoxide immediately prior to use. Zr(O^{n}Pr)$_4$ and [{Zr(O^{i}Pr)$_4$(^{i}PrOH)$_2$}] were purchased from Sigma Aldrich, and (TBA)$_2$-[WO_4],[41] $WO(OMe)_4$,[13] and [{Zr(O^{i}Pr)$_3$(O^{n}Pr)(^{i}PrOH)$_2$}][42] were prepared as described previously. 10% ^{17}O enriched water and deuterated acetonitrile were purchased from Goss Scientific Instruments. Infrared spectra were recorded either as Nujol mulls between KBr plates on a Mattson Genesis spectrometer or as powders on a Nicolet Avatar 370 DTGS spectrometer using a Smart Orbit single reflectance ATR attachment. ^{17}O NMR spectra were recorded at 67.63 MHz on a Jeol Lamda 500 spectrometer, and ^{183}W NMR spectra were recorded at 12.48 MHz on a Bruker Avance 300 spectrometer. ^{1}H NMR spectra were recorded at either 500.00 or 300.00 MHz, and ^{13}C-{^{1}H} NMR spectra, at either 125.65 or 75.39 MHz on a Jeol Lamda 500 or Bruker Avance 300 spectrometer, respectively. Resonances due to N^{n}Bu$_4^+$ cations are not listed but appear as multiplets centered at about 1.0, 1.4, 1.7, and 3.2 ppm in ^{1}H NMR spectra and as singlets at about 13, 19, 24, and 58 ppm in ^{13}C−{^{1}H} NMR spectra. Elemental and ESIMS analyses were performed by Newcastle University Chemical Analysis Service. Cyclic voltammetric measurements were made on 0.005 M samples with an AD Instruments potentiostat and MacLab 2e using a conventional three-electrode cell with a gold disc working electrode, platinum mesh auxiliary electrode, and a silver wire quasi-reference electrode. Ferrocene was added to the sample solution as a reference after completion of the measurements. A solution of (TBA)BF_4 in dried and degassed acetonitrile (0.05 M) was used as the supporting electrolyte.

X-ray Crystallography. Data were collected on Bruker SMART 1K CCD diffractometers using either a laboratory sealed-tube Mo Kα source or synchrotron radiation at station 9.8 of the UK Synchrotron Radiation Source, Daresbury Laboratory. Semiempirical absorption corrections, together with frame-scaling for intensity variations, particularly for synchrotron beam decay, were made on the basis of repeated and symmetry-equivalent reflections.[43] The structures were solved by standard direct methods and refined by full-matrix least-squares on all unique F^2 values.[44] Restraints were applied to molecular geometry and anisotropic displacement parameters of the lighter atoms, especially in cases of disorder. Hydrogen atoms, except for those for which positions are not uniquely dictated by purely geometrical considerations (e.g., those of acetonitrile molecules), were placed in idealized positions and refined as riding.

The salt of **1** gave non-merohedrally twinned crystals (ratio 82:18%), preventing the merging of symmetry-equivalent reflections before refinement. It also contained highly disordered solvent molecules; the effect on the diffraction pattern was treated by the SQUEEZE procedure of the program PLATON.[45] The dimeric anion has crystallographic inversion symmetry. The salt of **4** was pseudo-merohedrally twinned (91:9%) and showed end-to-end disorder of the ZrOPh group with the opposite WO group (57:43%), the two components being crystallographically independent. The salt of **5** was probably twinned, but this could not be resolved, leading to relatively high *R* factors; the anion has crystallographic mirror symmetry. Unresolved twinning is also likely for the salt of **6**, which showed disorder of WO and Zr(sal) for one of the two crystallographically independent anions (51:49%), with an unresolved disorder of solvent probably also involved. The salt of **7** was pseudo-merohedrally twinned (81:19%) and has two crystallographically independent anions in the asymmetric unit. The salt of **8** may have a small amount of unresolved twinning and has a disorder of WO and ZrOAc (75:25%), involving also disordered solvent. The very large structure of the salt of **9** contains two anions in the asymmetric unit, and it is possible that only some of the solvent present has been located and modeled. Satisfactory absolute structure parameters were refined for the noncentrosymmetric structures for **7** and **9**.[46]

[TBA]$_6$[{(MeO)ZrW_5O_{18}}$_2$], [TBA]$_6$1. A. Zr(O^{n}Pr)$_4$ (70% solution in *n*-propanol, 1.80 g, 5.49 mmol) in acetonitrile (20 mL) was heated to 90 °C and then added to a solution of (TBA)$_2$[WO_4] (4.47 g, 6.09 mmol) and $WO(OMe)_4$ (4.67 g, 14.40 mmol) in acetonitrile (20 mL) with stirring. The reaction mixture was heated to 90 °C for 3 h before addition of H_2O (10% ^{17}O-enriched, 622 μL, 34.43 mmol). After a further 3 h, MeOH (1 mL) was added and the solution was stirred for 12 h at 90 °C. After cooling to room temperature, the volume was reduced by 50% under reduced pressure and a small amount of crystalline (TBA)$_2$[W_6O_{19}] was removed by filtration before addition of an ether layer. The colorless crystals formed upon diffusion at −20 °C were filtered, washed with ether, and dried *in vacuo*. Yield 5.53 g, 63.4%.

B. Acetonitrile (30 mL) was added to [Zr(O^{i}Pr)$_4$(^{i}PrOH)$_2$}] (0.75 g, 0.97 mmol) with heating to 80 °C. A solution of (TBA)$_2$[WO_4] (2.12 g, 2.90 mmol) and $WO(OMe)_4$ (2.19 g, 6.77 mmol) in acetonitrile (15 mL) was added, and the mixture was heated at 80 °C for 3 h before addition of H_2O (10% ^{17}O-enriched, 296 μL, 16.45 mmol). After heating overnight at 80 °C, MeOH (5 mL) was added and after 2 h at 80 °C volatiles were removed. The residue was dissolved in acetonitrile (20 mL) and MeOH (5 mL) with heating at 80 °C for 2 h. After cooling to room temperature, the solution was filtered to remove an off-white solid, and the volume was reduced until crystals began to form. Cooling to −20 °C gave colorless needles (0.27 g) which were filtered off and washed with ether. After reduction of the solution volume, addition of ether and cooling to −20 °C gave further fractions. Total yield 2.31 g, 57%.

C. [{Zr(O^{i}Pr)$_3$(O^{n}Pr)(^{i}PrOH)$_2$}] (1.13 g, 1.45 mmol) was dissolved in a mixture of acetonitrile (40 mL) and toluene (10 mL) with heating to 80 °C, and a solution of (TBA)$_2$[WO_4] (3.18 g, 4.36 mmol) and $WO(OMe)_4$ (3.29 g, 10.16 mmol) in acetonitrile (15 mL) was added with stirring at 80 °C for 3.5 h before addition of H_2O (10%

(40) Errington, R. J. *Advanced Practical Inorganic and Metalorganic Chemistry*; Blackie Academic & Professional: London, 1997.
(41) Che, T. M.; Day, V. M.; Francesconi, L. C.; Fredrich, M. F.; Klemperer, W. G. *Inorg. Chem.* **1985**, *24*, 4055−4062.
(42) Seisenbaeva, G. A.; Gohil, S.; Kessler, V. *J. Mater. Chem.* **2004**, *14*, 3177−3190.
(43) Programs for data collection and processing were Bruker SMART, SAINT, and SADABS.
(44) Programs for structure solution and refinement were components of Bruker SHELXTL. Structure graphics were produced using either Bruker SHELXTL or CrystalMaker.
(45) Spek, A. L. *J. Appl. Crystallogr.* **2003**, *36*, 7−13.
(46) Flack, H. D. *Acta Crystallogr., Sect. A* **1983**, *39*, 876−881.

^{17}O-enriched, 444 μL, 24.67 mmol) and heating overnight. MeOH (7 mL) was added, and after heating at 90 °C for 5 h, volatiles were removed, the residue was dissolved in acetonitrile, and MeOH (7 mL) was added. After heating at 80 °C for 2 h the solution was filtered and evaporated to dryness. Recrystallization from acetonitrile−ether gave colorless crystals (3.97 g, 68%). ^{1}H NMR (500.0 MHz, CD_3CN): δ 3.75 (6H, OMe). ^{13}C NMR (125.7 MHz, CD_3CN): δ 59.1. FTIR: 1151m, 1106w, 1056w, 1031m, 964w, 946s, 898m, 884sh, 792s, 723s, 630, 536m, 487m, 456m, 418s cm^{-1}. Elemental Analysis Calcd for $C_{98}H_{222}N_6O_{38}W_{10}Zr_2$: C, 28.61; H, 5.44; N, 2.04%. Found: C, 28.57; H, 5.56; N, 2.15%.

2D EXSY NMR Study of Exchange of MeOH with (TBA)$_6$1. A sample for 2D EXSY ^{1}H NMR was prepared by adding methanol (*ca.* 5 μL, 0.12 mmol) to a solution of (TBA)$_6$**1** (0.05 g, 0.012 mmol) in CD_3CN. Two-dimensional proton EXSY spectra were obtained at 500 MHz using a 90° - t_1 - 90° - τ_{mix} - 90° - Acq(t_2) with appropriate phase-cycling to give a phase sensitive spectrum. The initial 512(t_2) × 128-(t_2) data matrix was zero-filled to 1024 × 512 points prior to Fourier transformation. Spectra were obtained with mixing times (τ_{mix}) of 200 and 350 ms, and the program EXSYCalc[47] was used to calculate exchange rates from the intensities of the diagonal and off-diagonal peaks.

Hydrolysis Study of (TBA)$_6$1. A. The ^{1}H NMR spectrum (300.1 MHz, CD_3CN) of a sample prepared from (TBA)$_6$**1** (0.075 g, 0.018 mmol) and H_2O (10% ^{17}O-enriched, 0.65 μL, 0.036 mmol) was recorded immediately after mixing and again after heating for 1 and 3 h at 80 °C. The sample was then transferred to a Schlenk flask and heated at 90 °C for 4.5 h. Volatiles were removed *in vacuo*, the sample was redissolved in CD_3CN, and the ^{1}H NMR spectrum was recorded. After evaporation to dryness, the residue was treated with MeOH (0.5 mL) at 70−80 °C for 4 h, stripped dry, and redissolved in CD_3CN and the ^{1}H NMR spectrum was recorded (see Figure 3).

B. H_2O (10% ^{17}O-enriched, 100 μL, 5.56 mmol) was added to (TBA)$_6$**1** (0.60 g, 0.146 mmol) in acetonitrile (15 mL). The mixture was stirred for 67 h at 70−80 °C, evaporated to dryness, and washed with ether (2 × 20 mL). Yield 0.54 g. Diffusion of an ether layer (1 mL) into an acetonitrile solution (3 mL) at −20 °C gave a small number of colorless crystals of (TBA)$_{12}$**3**·[W_6O_{19}][$W_{10}O_{32}$].

[TBA]$_6$[{(HO)ZrW$_5$O$_{18}$}$_2$], [TBA]$_6$3. (TBA)$_6$**1** (0.46 g, 0.11 mmol) in acetonitrile (5 mL) was treated with H_2O (0.4 mL, 22.36 mmol) and heated to 60 °C for 30 min. Volatiles were removed, the residue was dissolved in acetonitrile (5 mL), and the treatment with water was repeated twice more before evaporation to dryness. The solid was washed with diethyl ether (5 mL), dried *in vacuo*, and then dissolved in a hot mixture of acetonitrile (2 mL) and diethyl ether (5 mL). Crystals formed on cooling were filtered, washed with ether (3 × 5 mL), and pumped dry. Yield 0.39 g, 85%). Single crystals for X-ray crystallography were obtained from acetonitrile−ether. ^{1}H NMR (300.1 MHz, CD_3CN): δ 4.43 (2H, OH). FTIR: 3677w, 1647w, 1153w, 1107w, 1065w, 1028w, 967w, 942s, 882m, 797s, 723s, 634m, 555m, 412s cm^{-1}. Elemental Analysis Calcd for $C_{96}H_{218}N_6O_{38}W_{10}Zr_2$: C, 28.22; H, 5.38; N, 2.06%. Found: C, 28.34; H, 5.15; N, 2.06%.

(TBA)$_3$[(C$_6$H$_5$O)ZrW$_5$O$_{18}$], (TBA)$_3$4. Phenol (0.07 g, 0.70 mmol) was added to (TBA)$_6$**1** (0.54 g, 0.13 mmol) in acetonitrile (15 mL), and the reaction mixture was stirred at 90 °C for 16 h. The resulting yellow solution was evaporated to dryness, washed with toluene (2 × 20 mL) and ether (2 × 20 mL), and dried *in vacuo*. Yield 0.51 g, 92%. ^{1}H NMR (500.0 MHz, CD_3CN): δ 7.15 (m, 2H), 6.75 (br, 3H). ^{13}C NMR (125.7 MHz, CD_3CN): δ 130.1, 129.2, 120.1, 119.8. FTIR: 1592m, 1292s, 1152m, 1106w, 1066w, 1026w, 969sh, 953s, 907w, 876w, 785s (br), 730s, 693w, 627w, 607w, 565w, 427s cm^{-1}. Elemental Analysis Calcd for $C_{54}H_{69}N_3O_{18}W_5Zr$: C, 30.61; H, 5.38; N, 1.98%. Found: C, 30.21; H, 5.47; N, 2.00%.

(TBA)$_3$[(4-MeC$_6$H$_4$O)ZrW$_5$O$_{18}$], (TBA)$_3$5. (TBA)$_6$**1** (0.53 g, 0.13 mmol) was reacted with *p*-cresol (60 μL, 0.55 mmol) in acetonitrile (15 mL) at 90 °C for 49 h. The reaction solution was evaporated to dryness, and the remaining phenol was removed by washing with toluene and ether. Yield 0.49 g, 92%. ^{1}H NMR (500.0 MHz, CD_3CN): δ 7.0 − 6.9 (br d, 2H), 6.7−6.6 (br d, 2H), 2.21 (s, 3H, CH_3). ^{13}C NMR (125.7 MHz, CD_3CN): δ 130.5, 128.8, 119.8, 20.6. FTIR: 1507m, 1275s, 1152m, 1057w, 1027w, 969w, 954s, 787s, 730s, 627w, 564m, 416m cm^{-1}. Elemental Analysis Calcd for $C_{55}H_{71}N_3O_{18}W_5Zr$: C, 30.97; H, 5.43; N, 1.97%. Found: C, 29.96; H, 5.39; N, 1.98%.

5.9. (TBA)$_3$[{2-(CHO)C$_6$H$_4$O}ZrW$_5$O$_{18}$], (TBA)$_3$6. Salicylaldehyde (150 μL, 1.23 mmol) was added to a solution of (TBA)$_6$**1** (0.80 g, 0.195 mmol) in acetonitrile (15 mL), and the mixture was stirred at 70−75 °C for 24 h. The resulting yellow solution was evaporated to dryness, and the residue was washed with ether (2 × 20 mL) and dried *in vacuo*. Yield 0.79 g, 95%. ^{1}H NMR (500.0 MHz, CD_3CN): δ 9.66 (br s, 1H, CHO), 7.60−7.50 (m, 2H) 6.82−6.72 (br m, 2H). ^{13}C NMR (125.7 MHz, CD_3CN): δ 194.5, 139.7, 135.8, 124.2, 122.0. FTIR: 1636s, 1530m, 1194w, 1146m, 1024w, 964w, 944s, 903m, 802s, 772s, 730s, 661m, 615w, 596m, 554m, 469m cm^{-1}. Elemental Analysis Calcd for $C_{55}H_{71}N_3O_{18}W_5Zr$: C, 30.77; H, 5.31; N, 1.96%. Found: C, 31.10; H, 5.30; N, 2.06%.

(TBA)$_3$[(acac)Zr(W$_5$O$_{18}$)], (TBA)$_3$7. (TBA)$_6$**1** (1.41 g, 0.34 mmol) was reacted with acetylacetone (70 μL, 0.70 mmol) in acetonitrile (10 mL) at 85 °C for 21 h, during which time the solution changed from colorless to pale yellow. The volume was reduced by 50% *in vacuo*, and after separation of a small amount of (TBA)$_2$[W_6O_{19}], diffusion of an ether layer into the solution gave the crystalline product, which was isolated by filtration and washed with ether. Yield 1.28 g. 87.6%. ^{1}H NMR (500.0 MHz, CD_3CN): δ 5.69 (s, 1H, CH) 1.99 (s, 6H, CH_3). ^{13}C NMR (125.7 MHz, CD_3CN): δ 191.1, 103.8, 26.9. FTIR: 1673m, 1596s, 1526m, 1151s, 1105w, 1054w, 1024s, 9690sh, 944s, 896s, 800s (br), 769s, 730m, 655w, 551m cm^{-1}. Elemental Analysis Calcd for $C_{55}H_{71}N_3O_{18}W_5Zr$: C, 29.96; H, 5.45; N, 1.98%. Found: C, 29.81; H, 5.66; N, 2.04%.

(TBA)$_3$[(CH$_3$CO$_2$)Zr(W$_5$O$_{18}$)], (TBA)$_3$8. Acetic acid (200 μL, 3.33 mmol) was added to a solution of (TBA)$_6$**1** (0.60 g, 0.146 mmol) in acetonitrile (15 mL), and the mixture was heated at 75−76 °C for 19 h. The reaction mixture was evaporated to dryness, and the residue was washed with ether (2 × 20 mL) and dried *in vacuo*. Yield 0.53 g, 87%. ^{1}H NMR (500.0 MHz, CD_3CN): δ 1.96 (s, 3H, CH_3). ^{13}C NMR (125.7 MHz, CD_3CN): δ 21.9. FTIR: 1153m, 1106w, 1052w, 1025w, 970w, 950s, 904w, 887m, 804s (br), 734m, 692m, 619w, 563w, 426m cm^{-1}. Elemental Analysis Calcd for $C_{55}H_{71}N_3O_{18}W_5Zr$: C, 28.81; H, 5.37; N, 2.02%. Found: C, 28.70; H, 5.36; N, 2.02%.

Reaction between (TBA)$_6$1 and Ph$_2$PO$_2$H. Ph_2PO_2H (0.12 g, 0.55 mmol) was added to a solution of (TBA)$_6$**1** (0.74 g, 0.18 mmol) in acetonitrile (15 mL), and the mixture was heated at 72 °C for 21 h. Volatiles were removed, and the residue was washed with tetrahydrofuran (20 mL) and ether (2 × 20 mL) and dried *in vacuo*. Yield 0.72 g. ^{1}H NMR (500.0 MHz, CD_3CN): δ 8.11 (br, m), 7.41 (br, m), 7.18 (br, s), C_6H_5. ^{13}C NMR (125.7 MHz, CD_3CN): δ 133.6, 130.8, 128.6, 128.5. FTIR: 3054w, 2960m, 2932m, 2872m, 1644w, 1593w, 1481m, 1471m, 1463m, 1438m, 1379m, 1194m, 1127m, 1043w, 1014m, 995w, 945s, 902w, 779s, 752s, 723s, 695s, 625w, 550m, 411s cm^{-1}. Elemental Analysis Calcd for $C_{60}H_{118}N_3O_{20}PW_5Zr$: C, 32.13; H, 5.30; N, 1.87%. Found: C, 31.39; H, 5.38; N, 1.87%.

Several crystals of (TBA)$_7$**9** for X-ray diffraction were obtained by recrystallization of the crude product from acetonitrile (3 mL) by addition of an ether layer (2 mL) and diffusion at −20 °C. Insufficient material was obtained for elemental microanalysis.

Acknowledgment. We thank the EPSRC and Newcastle University for funding and the CCLRC (now STFC) for access to SRS facilities, staffing, and equipment funding. We are also grateful to Bruker AXS for a CASE award (RAC).

(47) Zolnai, Z.; Juranic, N.; Vikic-Topic, D.; Macura, S. *J. Chem. Inf. Comput. Sci.* **2000**, *40*, 611−621.

Supporting Information Available: ESI mass spectrum of $(TBA)_6$**3**, FTIR and ^{17}O NMR spectra of the products from reactions between $(TBA)_6$**1** and HBF_4, structural diagrams with thermal ellipsoids, tables of bond lengths and angles and crystallographic CIF files. This material is available free of charge via the Internet at http://pubs.acs.org.

JA0725495